Mohamed Khider University of Biskra
Faculty of exact sciences and natural and life sciences
Material sciences department

MASTER MEMORY

Matter sciences
Physics
Material physics
Réf. : Entrez la référence du document

Presented by:
Djohina
Bendjaballah
Le :

Study of CuSCN material effect on perovskite solar cell

Jury:

Mr.	Boumaaraf Rami	MCB	University of Biskra	President
Mme	Laiadi widad	MCA	University of Biskra	Supervisor
Mme	Ouamane Samia	MCB	University of Biskra	Examiner

AcademicYear: 2022/2023

Table of contents

Table of contents

Table of contents

Table of contents

Didacation

This dissertation is dedicated to my family that supported me

To my best mother ‘’Reugia ‘’

To my best father ‘’Sebti’’

To my grand mother ‘’Sghira’’

To my brother ‘’Mohamed’’ ‘’Belkacem’’

To my sister ‘’Meriem’’

To my brother wife ‘’ Somia’’

To my Fiance ‘’Chadli’’

To my best freinds ‘’Imene, Amira, Salsabil,

Amina, Bouthina, Ilhame, kaouthar, romissa, Fedia, Fatima……

To my loved ones ‘’Jouda’’ ‘’Firas’’ ‘’Abdou’’ ‘’Amine’’ ‘’ Sadja’’ ‘’Nada’’

Knowledgemets

Thank first and foremost to Allah,

Without his never have been finished on time

Then we should thank everyone who contributed to the success of this work. Foremost my utmost gratitude goes to my supervisor,

M^{me}. Widad Laiadi to whom I would express my sincere thanks.

I am very grateful for her support,

her patience in completing this study

In addition to our consultant, I would like to thank

jury members, M^{r} Boumaaraf Rami, as president and

M^{me}. Ouamen Samia as examinater

Abstract

The main objective of this work is to study CuSCN material effect on perovskite solar cells, using SILVACO simulation software. We presented a theoretical part that contains basic concepts about perovskite solar cells in general, the simulation allowed to study the effect of the PEDOT: PSS material on the electrical property (I-V). We studied the effect of replacing PEDOT: PSS with CuSCN material this study proved that CuSCN material improved the output parameters of the perovskite solar cells, after that we studied the effect of the doping concentration of CuScN layer on the electrical properties of the solar cells, an important result which obtained also of this study is doping concentration of CuScN layer improved the electrical property (IV), and the electrical properties of the perovskite solar cell.

Keywords: Perovskite, MAPbI3, Silvaco, HTL, CuSCN

Résumé

L'objectif principal de ce travail est d'étudier l'effet du matériau CuSCN sur les cellules solaires à pérovskite, on utilisant le logiciel de simulation SILVACO.
Nous avons présenté une partie théorique qui contient des concepts de base sur les cellules solaires à pérovskite en général. La simulation nous a permis d'étudier l'effet du matériau PEDOT : PSS sur la propriété électrique (I-V). Nous avons étudié l'effet du remplacement de PEDOT: PSS par le matériau CuSCN, cette étude a prouvé que le matériau CuSCN améliorait les paramètres de sortie des cellules solaires en pérovskite, après cela, nous avons étudié l'effet de la concentration de dopage de la couche CuScN sur les propriétés électriques des cellules solaires, un résultat important obtenu également de cette étude est la concentration de dopage de la couche de CuScN qui a amélioré la propriété électrique (IV) et les propriétés électriques de la cellule solaire pérovskite.

Mot clé : Perovskite, MAPbI3, Silvaco, HTL, CuSCN

List of figures

List of figures

List of figures

List of tables

List of abbreviations

PV	Photovoltaic
λ	Wavelength
I	Total current
I0	Saturation current
Q	Electronic charge
η	Ideality factor
T	Environnment temperature
J-V	Current –density vs.voltage
Jsc	short circuit current
V0c	Open circuit voltage
FF	Fill factor
PCE	Power conversion efficiency
PCE	Perovskite solar cell
ETL	Electron transport layer
HTL	Hole transport layer
ETM	Electron transport material
FTO	Fluorine-doped tin oxide
CuSCN	Copper(I) thiocyanate
Tio2	Titanium dioxide
CH3NH3I3	Organic components

List of abbreviations

VASP	Vacuum-assisted solution process
MAPbI3	Methylamo,ium lead iodide
C	Light speed
H	Planck ‘s constant
Silvaco	Silicon valley comporation
DDSS	Dye-sensitized solar cells
CuSCN	copper(I) thiocyanate
I	Iodide
Pb	Lead
OPV	Organic photovolraic
CIGS	copper-Indium-Gallium-Selenide
CdTe	Cadmium Telluride
IQE	Internal Quantum Efficiency
EQE	External Quantum Efficiency
QE	Quantum Efficiency

Introduction

Introduction

Energy is one of the basic elements of modernization and urbanization because of industrialization, Due to the growing prosperity of emerging countries, energy demand is growing rapidly. The default choice to meet this demand is fossil fuels. The increase in energy demand has brought about this Depletion of the world's fossil fuel resources. In addition, the consumption of fossil energy has produced harmful side effects of greenhouse gases, which has led to an Atmospheric carbon dioxide concentration increase and global warming. Research on renewable energy and environmentally friendly alternatives to fossil fuels is one of the most important goals of energy production. In particular, one of the most promising renewable energy sources is solar PV. Photovoltaics (PV) is a technology that utilizes semiconductor materials exhibits the photovoltaic effect and converts sunlight into usable electricity, especially most promising is that solar energy is non-polluting in everyday use. The rapid improvement of perovskite solar cells has made them a rising star in the field of photovoltaics, arousing great interest in academia. Since their method of operation is still relatively new, there is a great opportunity to further explore the fundamental physics and chemistry surrounding perovskite. Furthermore, it has been shown in recent years that technological improvements in perovskite formulation and manufacturing procedures lead to significant increases in power conversion efficiency [1]. The terms ''perovskite'' and'' perovskite structure'' are often used interchangeably. Technically, perovskite is a mineral first discovered in the Urals and named after lev perovsky (founder of the Russian Geographical Society). A perovskite structure is any compound that has the same structure as the perovskite mineral.

Although perovskites come from a seemingly different crystallographic world, they can be easily integrated into thin-film architectures. The first perovskite solar cells were based on solid-state dye solar cells (DSSCs), Thus using a TiO_2 framework. Since then, many cells have followed this template or used an Al_2O_3 framework in a ''mesoscopic superstructure'' architecture, but the high-temperature steps required for fabrication and the UV instability of TiO_2 have led to other ''planar'' architectures where thin cells use similar. Membrane cells. After lagging behind mesoporous cells in terms of efficiency for several years, planar perovskites are now nearly as efficient [1]. The perovskite films themselves are usually processed by vacuum or solution processes. Movie quality is very important. Initially, vacuum-deposited thin films provided the best equipment, but the process required the simultaneous evaporation of organic components (methylammonium) and inorganic components (lead halides) which required dedicated evaporation chambers that were not available to many

researchers. Consequently, considerable effort has been expended to improve solution-processed devices, as they are simpler, allow low-temperature processing, and are now comparable in efficiency to vacuum-processed cells [2].

Typically, the active layer of a perovskite solar cell is deposited via one of two processes. The first is a one-step process, in which a solution of precursors, such as PbI_2 and CH_3NH_3I, is coated and then heated to form the perovskite film. An alternative to this is the ‘’antisolvent’’ method, where the precursor solution is applied in a polar solvent and then rapidly cooled during the spin coating process with a non-polar solvent, Achieving optimal performance requires precise timing and volume control of the quenching solvents. To aid in this process, the authors of the literature [3] developed a series of syringe pumps that have helped them achieve in-house power conversion efficiency values of over 16% [3].

The work presented here is a study of CuScN material effect on perovskite solar cells, the first chapter gives an overview of perovskite solar cells technology, and solar cells characteristics. Chapter II focused on CuScN material and its properties. Moreover, the structure of organic-inorganic halide perovskite is presented, providing an insight into its composition. In order to influence both the optical and electrical properties, various manufacturing methods are taken into account. Chapter III summarizes the simulation software and the main parameters used. And discusses the results obtained in this work, drawing conclusions.

Chapter I
Perovskite solar cells

Chapter I: perovskite solar cells

I.1 Introduction

To meet the global energy demand and combat climate change, solar energy, one of the renewable energy sources, is becoming more and more crucial. Currently, one of the most rapidly developing renewable energy technologies, photovoltaic (PV) technology is poised to play a significant role in the mix of the world's future electricity generation [3].
Solar cells are a device that converts the energy of photons (light) into electrical energy released in the form of electric charge. It is directly exposed to the sun and absorbs light for conversion; Solar cells have many uses including satellites and they are used in many purposes and fields. In this chapter, we will get acquainted with solar cells in general, and we will present their working principles, as well as their characteristics.

I.2 Solar cells

Solar cells are devices in which sunlight releases electric charges so they can move freely in a semiconductor and ultimately flow through an electric load, such as a light bulb or a motor. The phenomenon of producing voltages and currents in this way is known as the photovoltaic effect [1]. The formation of both positive and negative charges, as well as a compelling force to push these charges via an external electric circuit for charge collection, are necessary to use the generated electricity, the external circuit can afterwards be linked to any electrical device. In fact, the photon that strikes the solar cell's electron must have sufficient energy to excite a valance electron and cause it to move into the conduction band. The probability that an electron will be in the conduction route and be useful for generating power is determined by the energy gap between the valance band and conduction band and the energy that the photon provides to the valance electron. The rate at which electrons are stimulated to move into the conduction band determines the maximum current. Converting solar light into electrical energy. With its minimal negative effects on the environment, low cost, and limitless high electromagnetic radiation to our planet, solar energy has a plethora of clear advantages. Additionally, it makes use of solar cells, which are safer, more effective, and cleaner than previous methods. Also, the direct conversion of solar energy into electricity results in a more effective energy transit and storage step. In a nutshell, the general goal of this technology is to maximize solar energy capture while maintaining a balance, nevertheless, this technique has been drawing significant interest since 1954, when Bell Laboratories developed the first contemporary p-n solar cell

utilizing silicon, with a reported effectiveness of 6%. Then, Si-based solar cell technology, which has a high efficiency (over 26% versus "modest" fabrication costs), dominates the contemporary PV market. This is because of effective advancements in both the technology's fundamental physical understanding and device engineering [4].

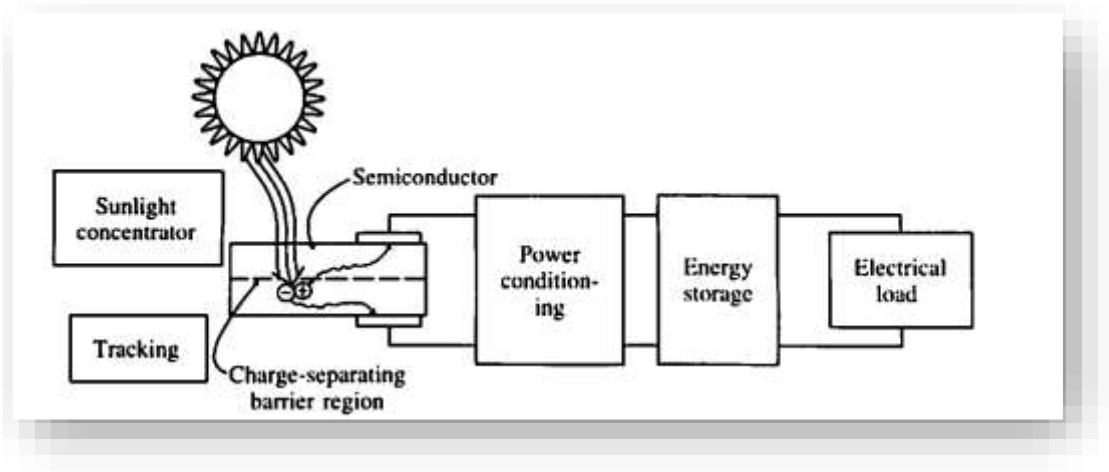

Figure I.1: Sketch showing functional elements of solar cell system.

I.3 Solar cells characteristics

I.3.1 Short circuit current

A short circuit current is the maximum current of a solar panel without a load connected. They are measures of the maximum current and voltage a solar panel can produce. It is the current that flows in the junction in case of a short circuit; it means when the resistance of the load is equal to zero and therefore the voltage applied to the link is equal to zero. It mainly depends on the number of incident photons as well as the spectrum area of the solar cell. Optical properties and the collection probability of photo general carriers [4].

All solar panels come with a short-circuit current rating. This is when the current in the solar panel is at its maximum and there is no voltage. In this case, there is no power coming from the solar panel because there is no voltage. To get power from a solar cell you need both current and voltage. Current (Amps) x Voltage (Volts) = Power (Watts).

Short circuit current is important because it's used to calculate the size of the conductors or wires you will use in your system. The short circuit current is also used to determine the size of the other components in the solar system such as the breakers for example.

The short circuit current is always given by the manufacturer on the back of the panel as the Isc and is expressed in amps (A).

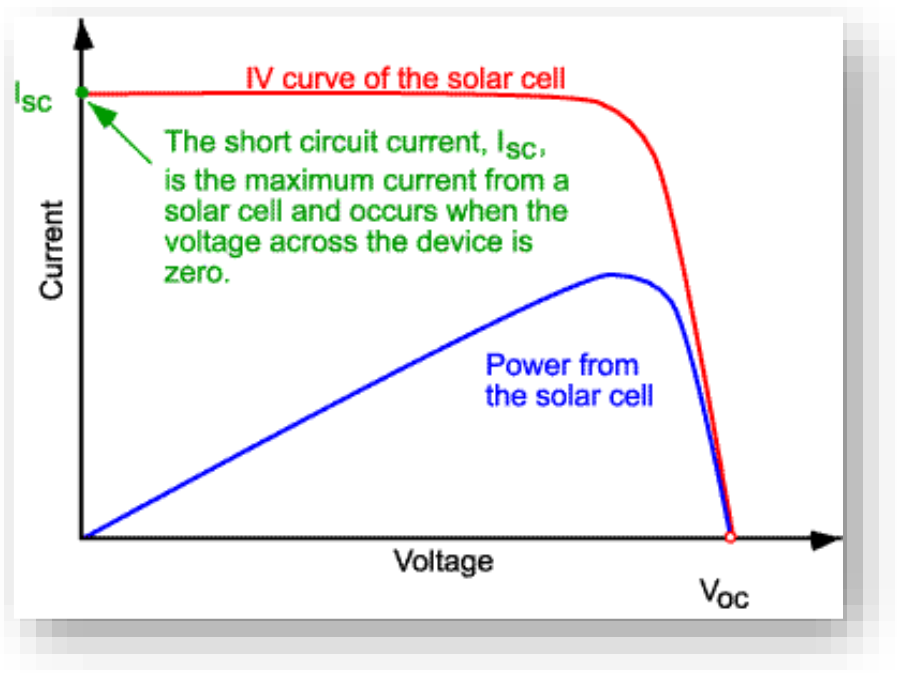

Figure I.2: I-V curve of a solar cell showing short circuit current.

I.3.2 open circuit voltage

In electrical and electronic circuits, the difference between potentials of two points is referred to as voltage or potential difference. Sometime we come across a term "open circuit voltage" while analyzing electric circuits. The term open circuit voltage is very common when we use Thevenin's Theorem to analyze the circuit. In an electric circuit, when a gap or open is created, and the difference of potentials between the two points of the open is referred to as the open circuit voltage. In circuit analysis terminology, we usually refer to the open circuit voltage as the Thevenin's Voltage because the calculation of the open circuit voltage is used in Thevenin's Theorem. The open circuit voltage is often represented by the symbol V_{OC}. The open circuit

voltage is commonly used to express the voltage or potential difference of solar cells and batteries.

When a solar cell is an open circuited, and no load is connected across the solar cell then current will be at its minimum (zero) value whereas the voltage will be at maximum value [5].

The produced voltage by the solar cell when no current flows is Voc. This occurs when the electric field due to the applied voltage cancels the built- in potential of the device [6]. The graphical representation of Voc is given in Figure I.3.

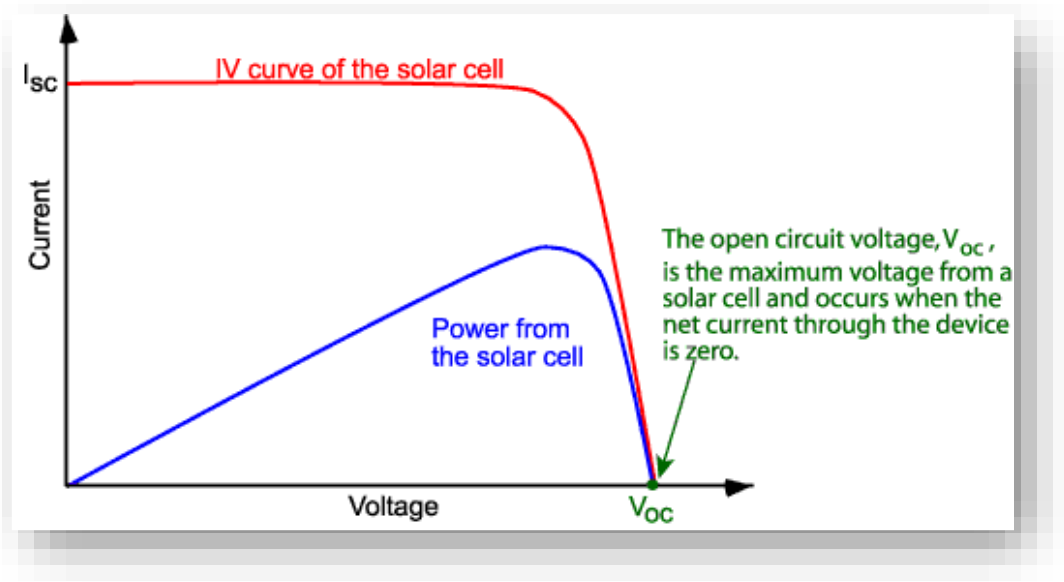

Figure I.3: I-V curve of a solar cell showing the open circuit voltage.

I.3.3 Fill factor

The fill factor (FF) is an important parameter that determines the power conversion efficiency of an organic solar cell. There are several factors that can significantly influence FF, and these factors interact with each other very intricately.

The fill factor is always below 1 and is high in value as good as the solar cell is. Good fill factors are typically approaching 80%, these high values are completely dependent on high shunt resistance and low series resistance [7].

The short-circuit current and the open-circuit voltage are the maximum current and voltage respectively from a solar cell. However, at both of these operating points, the power from the

solar cell is zero. The "Fill factor", more commonly known by its abbreviation "FF", is a parameter which, in conjunction with V_{oc} and I_{sc}, determines the maximum power from a solar cell. The FF is defined as the ratio of the maximum power from the solar cell to the product of V_{oc} and I_{sc}.

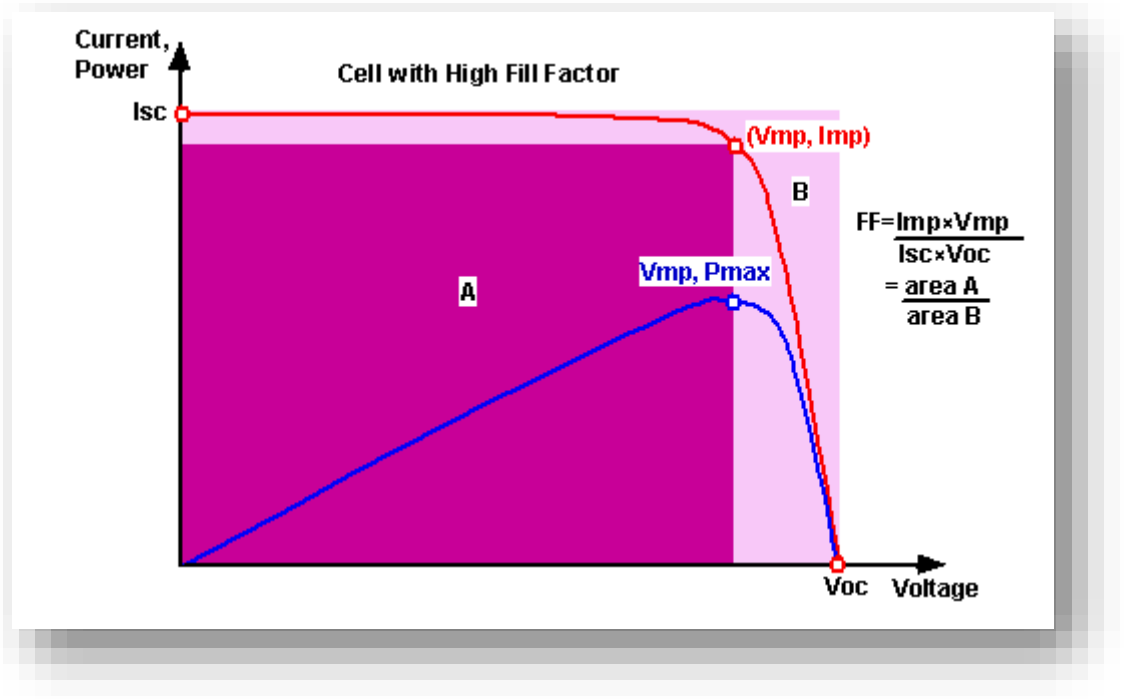

Figure I.4: typical current density-voltage curve.

I.3.4 Quantum Efficiency

It is the ratio of the number of free carriers given by the solar cell to the number of photons entering the solar cell from the outside. The 'quantum efficiency' (QE) certain wavelength is absorbed and the resulting minority carriers are collected, then the quantum efficiency at that particular wavelength is unity [3]. Quantum efficiency may be given either as a function of wavelength or of energy. If all photons of a certain wavelength are absorbed and the resulting minority carriers are collected, then the quantum efficiency at that particular wavelength is unity. The quantum efficiency for photons with energy below the band gap is zero.

Two types of quantum efficiency of a solar cell are often considered:

- **External Quantum Efficiency (EQE)** is the ratio of the number of charge carriers collected by the solar cell to the number of photons of a given energy shining on the solar cell from outside (incident photons).
- **Internal Quantum Efficiency (IQE)** is the ratio of the number of charge carriers collected by the solar cell to the number of photons of a given energy that shine on the solar cell from outside and are absorbed by the cell.

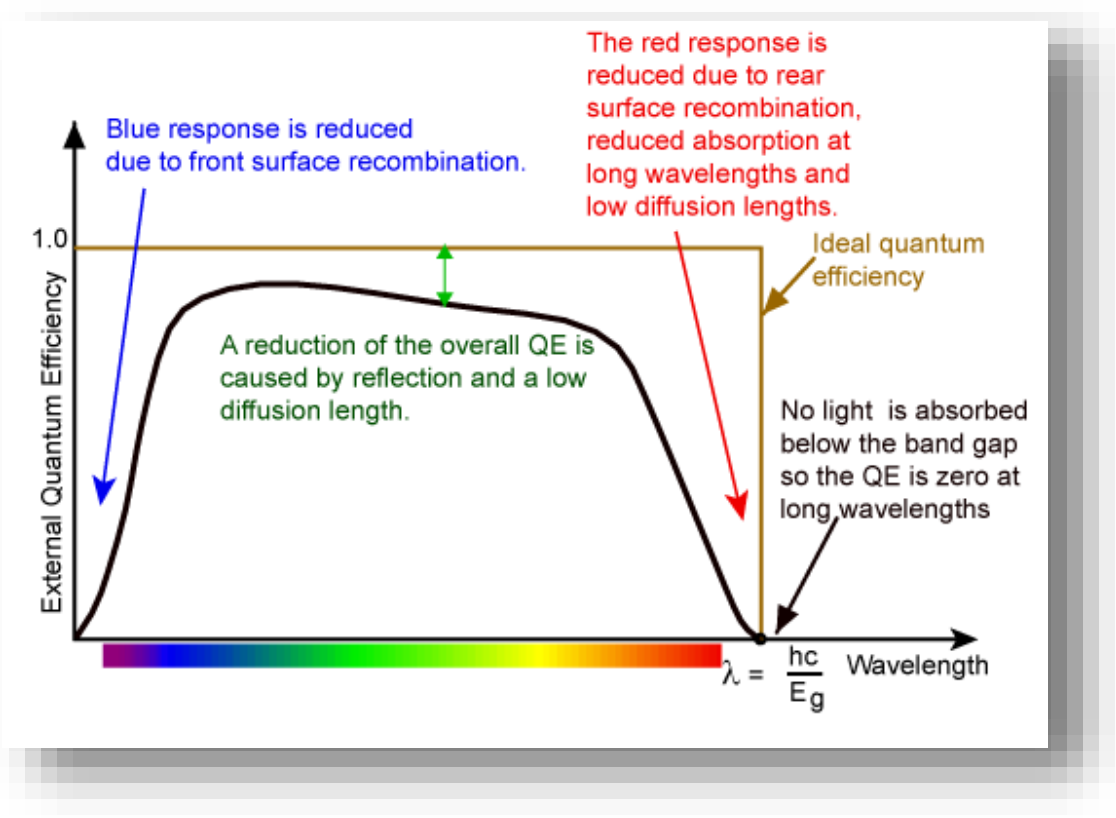

Figure I.5: the quantum efficiency of a silicon solar cell.

While quantum efficiency ideally has the square shape shown above, the quantum efficiency for most solar cells is reduced due to recombination effects. The same mechanisms which affect the collection probability also affect the quantum efficiency. For example, front surface passivation affects carriers generated near the surface, and since blue light is absorbed very close to the surface, high front surface recombination will affect the "blue" portion of the quantum efficiency. Similarly, green light is absorbed in the bulk of a solar cell and a low diffusion length will affect the collection probability from the solar cell bulk and reduce the

quantum efficiency in the green portion of the spectrum. The quantum efficiency can be viewed as the collection probability due the generation profile of a single wavelength, integrated over the device thickness and normalized to the incident number of photons at that wavelength.

I.3.5 Power conversion efficiency

The power conversion efficiency is the most important parameter of a solar cell, determined by the ratio of maximum extracted power relative to the incident power onto the solar cell [7].

I.4 Generation of solar cell

Over the past few decades, many new types of solar cells have been developed. There are three generations of solar cells [10]. The various photovoltaic technologies with the best power conversion efficiencies studied globally from 1976 to 2019 (see figure.III.6), this information sheet is published by the U.S. Department of Energy's National Renewable Energy Laboratory (NREL). The energy conversion efficiency of various types of solar cells has improved over time. The classification is based on the type of material, the maximum achievable efficiency and the cost of each type (Figure.I.7) [10].

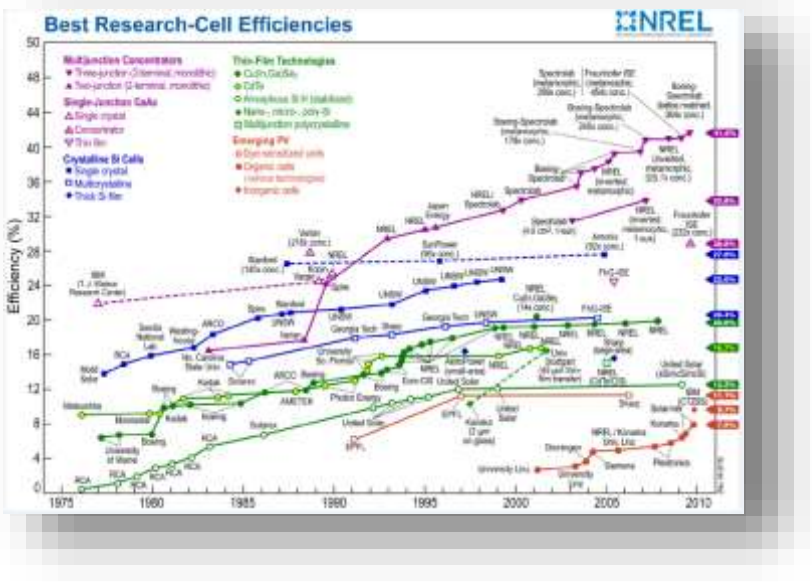

Figure I.6: Best research-cell efficiencies for the multitude of different solar cell technologies.

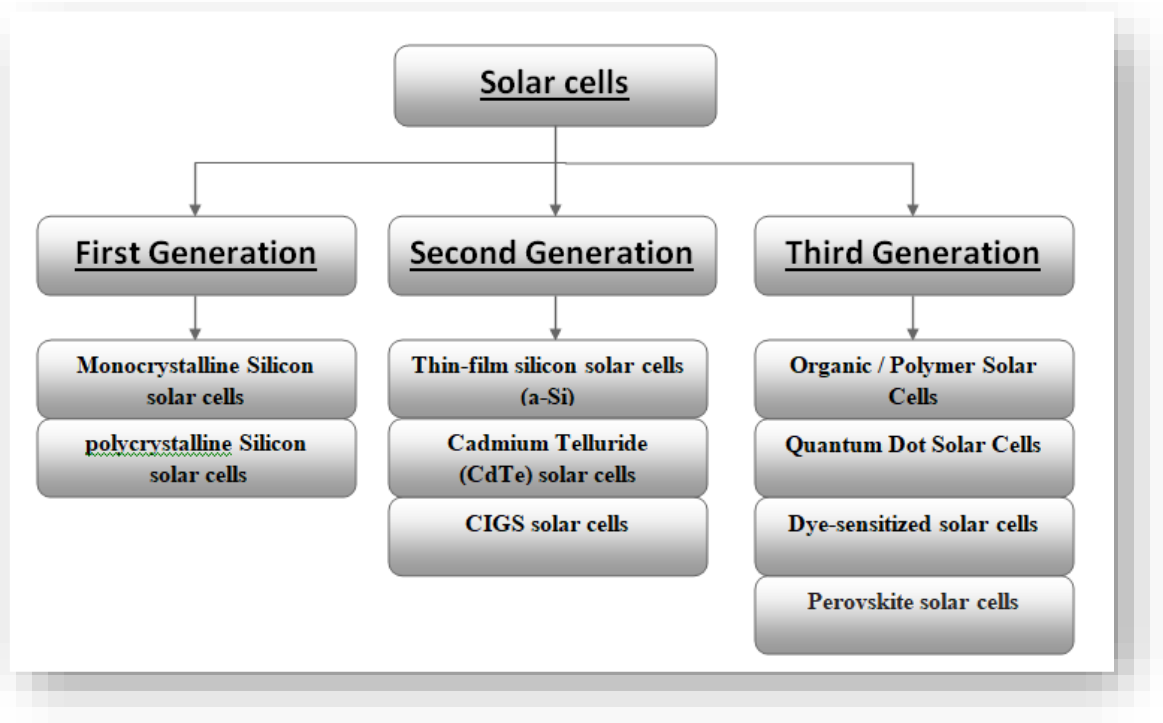

Figure I.7: Classification of various solar cell technology.

I.4.1 First generation

The first generation of solar cells is silicon solar cells, including polycrystalline silicon solar cells and monocrystalline silicon solar cells. They typically feature large-area, high-quality single-contact devices; they have a theoretical efficiency limit of 33% for a single contact [11] and [12].

I.4.1.1 Monocrystalline silicon

Monocrystalline solar cells consist of large single crystals of pure silicon. Such single crystals are mainly produced using the Czochralski method [13]. The efficiency of monocrystalline silicon solar cells is between 25% and 26% [14], however, this type of solar cells is very expensive because they are cut from cylindrical blocks and cannot completely cover square solar cell modules, resulting in a large amount of refined silicon is wasted [11].

I.4.1.2 Polycrystalline silicon

Polycrystalline silicon solar cells are the most popular solar cells at present, because the processing of polycrystalline silicon solar cells is more economical, and the battery module array is usually rectangular, but the purity of polycrystalline silicon is much lower than that of monocrystalline silicon. Silicon solar cells of this type have efficiencies between 20% and 22% [12] and [15] and [16].

I .4.2 Second generation

Second-generation solar cells are also called thin-film solar cells because they consist of layers a few microns thick. This generation of cells is much cheaper to produce than the first generation and promises higher efficiencies. Commercially developed thin-film solar cells basically fall into three main types [17] and [14].

I.4.2.1 Thin-Film silicon solar cells

Currently, amorphous and microcrystalline silicon are highly promising material choices for large-scale, cost-effective photovoltaic applications on Earth due to their ability to be fabricated using low-temperature processes such as PECVD [18].
Unlike c-Si solar cells that are based on wafers, amorphous silicon solar cells do not use a p-n junction. They instead rely on a p-i-n junction, which sandwiches an intrinsic layer between thin p- and n-doped layers to produce an electric field that aids in transporting the carriers. Utilizing tandem and even triple layer devices with p-i-n cells can enhance the performance of solar cells. 10% or below is the best stabilized module efficiency [4] and [17].

I.4.2.2 Thin-Film Cadmium telluride (CdTe) solar cells

The development of CdTe thin film cells has accelerated recently. Because of their ability to compete on price (the first PV technology at a low price), high conversion efficiency, and the availability of production techniques. In order to create a p-n junction diode, the CdTe solar cells are typically built by sandwiching between cadmium sulphide layers [15] and [19].
The CdTe is the most desirable material for thin-film solar cell design because it has a great direct band gap of 1.45 eV and a high absorption coefficient, resulting in an efficiency of 21.4%.

But because to the primary problems with poisonous Cd-based materials, this CdTe technology is constrained [12] and [16].

I.4.2.3 CIGS solar cells

The use of CIGS solar cells to produce solar energy is gaining popularity all over the world. They are regarded as the most promising cells because they demonstrated excellent stability in outdoor tests (without noticeably degrading) and because their conversion efficiency (23.35%) is nearly as high as that of poly-Si cells' conversion efficiency [16] and [20] and [21]. Thin film solar cells can be produced using the compound semiconductor copper-indium-gallium-selenide (CIGS) as the base material. It is a high absorption coefficient direct gap semiconductor [22].

I.4.3 Third generation

A new generation of solar cells evolved primarily as a result of the high cost of first generation solar cells, their toxicity, and the scarcity of resources for second generation solar cells. Because they do not rely on the p-n junction design of the other two generations, this generation is fundamentally distinct from them [23].

Of course, the ultimate goal is to enhance solar cells by making solar energy more effective over a wider range of solar energy, less expensive, and non-toxic. In order to reach these high efficiencies, numerous approaches have been researched in recent years. Organic thin film (polymer solar cells), dye-sensitized, perovskite, and quantum dot solar cells are among the solar cells in this generation [23] and [44].

I.4.3.1 Organic or Polymer solar cells

The potential of organic solar cells as solution- processable, lightweight, inexpensive, large-area energy producers, and more flexible solar cells is the subject of intense research. Because the active layers of the cell are made entirely of organic substances, such as polymers and small-molecule compounds, organic or polymer cells are categorized as such [25].

I.4.3.2 Quantum Dot solar cells

Quantum dots (QDs) can be shaped into many various forms, in two-dimensional (sheets) or three-dimensional arrays, and have the benefit of a tunable bandgap as a result of size variation and the development of intermediate bands. A photon typically produces one electron-hole pair. But several electron-hole pairs, often 2 or 3, can occur when a photon strikes a QD composed of the same semiconductor material, although 7 has occasionally been recorded. This technology's maximum theoretical efficiency is reportedly 63% [15] and [12] and [13].

I.4.3.3 Dye-sensitized solar cells

The DSSC device is made up of four parts: a counter electrode, a redox electrolyte, a dye sensitizer, and a semiconductor (see Figure I.8). Due to their high efficiency (12%), low cost, straightforward fabrication processes, environmental friendliness, transparency, and good flexibility, dye-sensitized solar cells exhibit distinct advantages over conventional photovoltaic technologies. However, there are certain difficulties, such as dye molecule breakdown in the presence of heat and UV light and problems with stability brought on by liquid electrolytes. The lifespan of DSSC is quite limited (five years) as a result of all these issues [26] and [14].

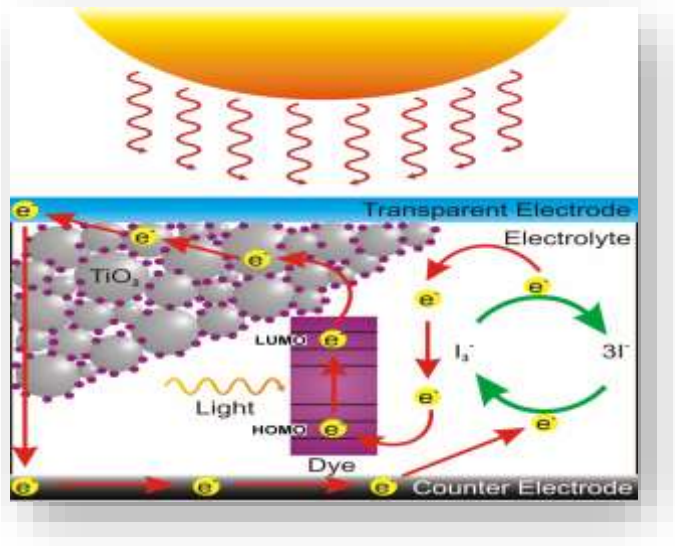

Figure I.8: Structure and operation of a dye-sensitized solar cell.

According to Figure I.8 the incident light excites anelectron in a dye molecule into a higher state. Such an excited electron tunnel onto a TiO_2 molecule. The electron then diffuses to the end of the electrode, enters the external circuit andre-enters the cell through the opposite electrode. The oxidized dye molecule is reduced by the electrolyte and the electrolyte is reduced by the re-entering electron [14].

I.5 Perovskite solar cells

The term "perovskite solar cell" refers to the ABX_3 crystal structure, also known as the perovskite structure, of the absorber materials, where A and B are cations and X is an anion. It has been discovered that cations can form perovskite structures [27]. Methyl ammonium lead trihalide ($CH_3NH_3PbX_3$, where X is a halogen ion like iodide, bromide, or chloride) is the most researched perovskite absorbed and has an optical bandgap ranging from 1.55 to 2.3 eV depending on the halide content. With a bandgap ranging from 1.48 to 2.2 eV, formamidinium lead trihalide ($H_2NCHNH_2PbX_3$) has also demonstrated that it is promising candidate. It should be able to achieve higher efficiencies than methyl ammonium lead trihalide because its minimum bandgap is closer to the ideal value for a single-junction cell [28].

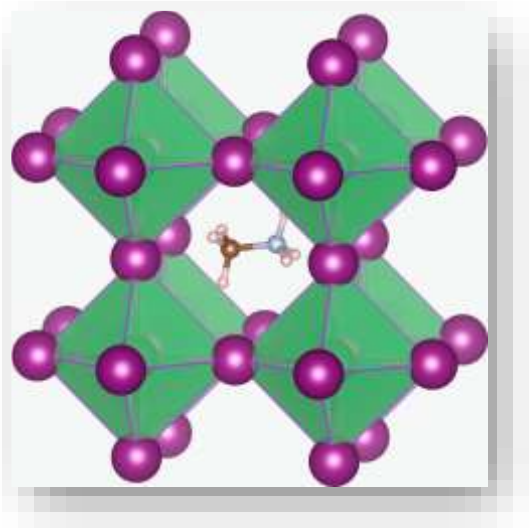

Figure I.9: Crystal structure of $CH_3NH_3PbX_3$ perovskite (X=I, Br and /or CI).

The methyl ammonium cation ($CH3NH3^{+}$) is surrounded by PbX6 octahedra [28]. Perovskite solar cells are a brand-new class of solar cells that have arisen within the past ten years. Dye-sensitized solar cells are the ancestor of perovskite solar cells. Solid-state sensitized solar cells, which are based on dye-sensitized Gratzel solar cells and perovskite, are the basis for this type of solar cell. A promising photovoltaic technique is solar cells. The rapid advancement in power conversion efficiency (PCE) of perovskite solar cells (PSCs), from the initial PCE of 3.8% in 2009 for the first prototype to the certified PCE of 25.2% in 2019 , has generated a great deal of interest [13, 25] In just about a decade, the photovoltaics of organic-inorganic lead halide perovskite materials have demonstrated rapid improvements in solar cell performance, surpassing the highest efficiency of semiconductor compounds used in solar cells, such as CdTe and CIGS (copper indium gallium selenide), though they still fall short of silicon photovoltaics, which hold a record-high efficiency of 26.6% [25].

I.5.1 Working principle of a perovskite solar cell

The solar cell produces light energy. The fundamental of a solar cell for converting solar energy into electric power is the generation of negative and positive charges in the active layer. The photovoltaic system has three main functioning steps [11]:

Absorption of photons, convert photon energy into electrical energy, Charge extraction. The external circuit can be later connected to any electrical equipment to utilize the generated electrical power. In fact the photon striking the electron in the solar cell must possess enough energy to excite a valance electron to jump to the conduction band [12].

For each layer, the energy levels should be thoroughly investigated. Since the excited electrons and holes are attempting to join again to reduce the overall energy. But because charge carriers are also energy-conserving, they always choose the route of least resistance. This is accomplished by making the level of the ETLs' LUMO (lower unoccupied molecular orbital) slightly lower than that of the active layers' LUMO, which provides an electron with a more desirable path to travel. The highest occupied molecular orbital, or HTLs HOMO, must be a little higher than the active layers HOMO in order to provide holes with a more desirable route to travel. Each layer in the cell either has a greater HOMO or a lower LUMO for the charge carriers' transportation chain, and this is true for all layers (Figure I.11) [25].

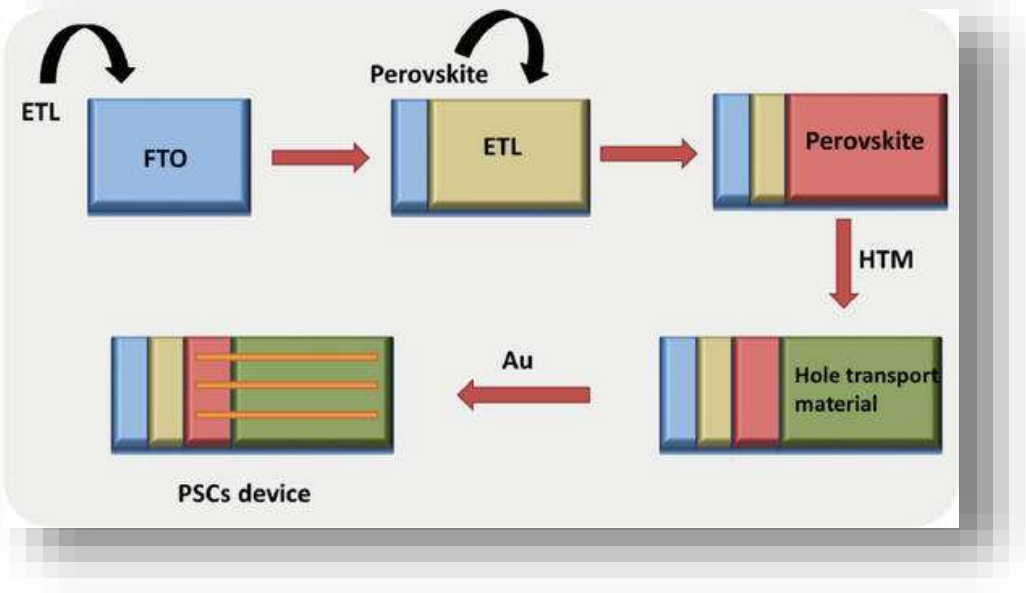

Figure I.10: general working principle of perovskite solar cells.

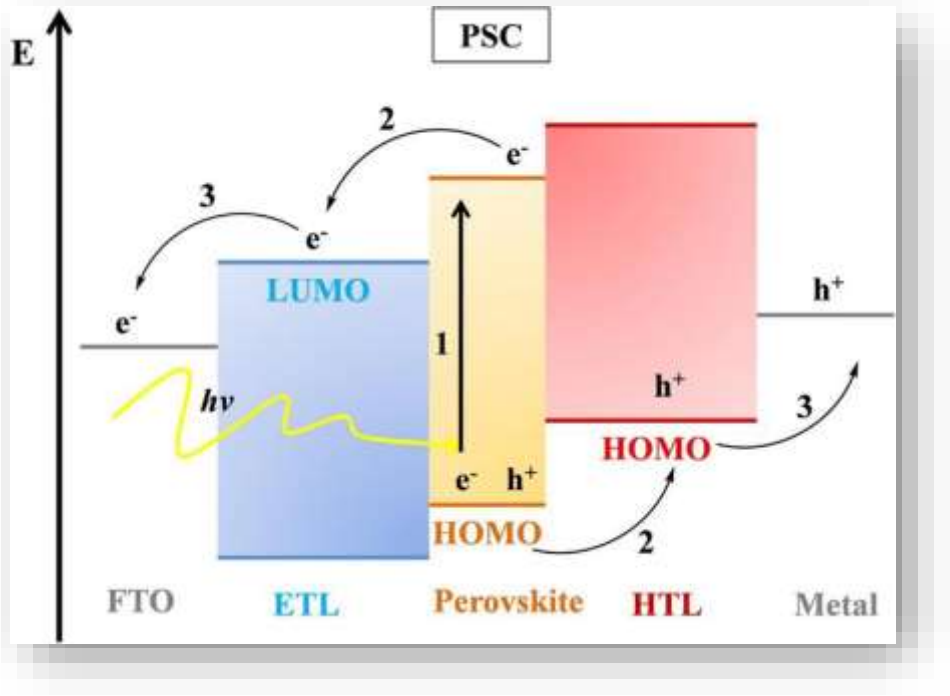

Figure I.11: Band diagram and operation principle of perovskite solar cell.

I.5.2 Perovskite solar cell device structure

Perovskite solar cells exhibit a series of distinctive features in their optoelectronic response that have a crucial influence on the performance, particularly for long-time response [14]

Where the planar architecture is an evolution of the mesoscopic structure, where the perovskite light-harvesting layer is sandwiched between the electron (ETM) and hole transporting materials (HTM) , the absence of a mesoporous metal oxide layer leads to an overall simpler structure [15].

When the liquid electrolyte was replaced with a solid-state substance known as mesoscopic device architectures, interest in perovskite solar cells grew and expanded [26, 29]. Where the perovskite light-harvesting layer is positioned between the electron (ETM) and hole carrying materials (HTM), the planar architecture is an extension of the mesoscopic structure (see Figure I.12.A).

The overall structure is simpler as a result of the lack of a mesoporous metal oxide layer. By carefully regulating the interfaces between the several layers that comprise the PSC (the perovskite light absorber layer, the electron transporting layer, the hole transporting layer, and the electrodes), it is possible to attain a high efficiency without the mesoporous layer [27, 28].

The n-i-p structure is known as the normal device structure (see Figure I.12.B) and the p-i-n structure is also known as the inverted device structure (see Figure I.12.C) of the planar device structure that was developed with the perovskite absorber sandwiched between the electron (ETM) and hole transporting materials (HTM). Simply speaking, depending on where the ETM and HTM are located [29, 30].

Additionally, in order to create effective n-i-p (normal planar) and p-i-n (inverted planar) hybrid architectures of PSCs, it is usually required to optimize each layer while retaining its charge mobility, electron balance, and optical transmittance [31].

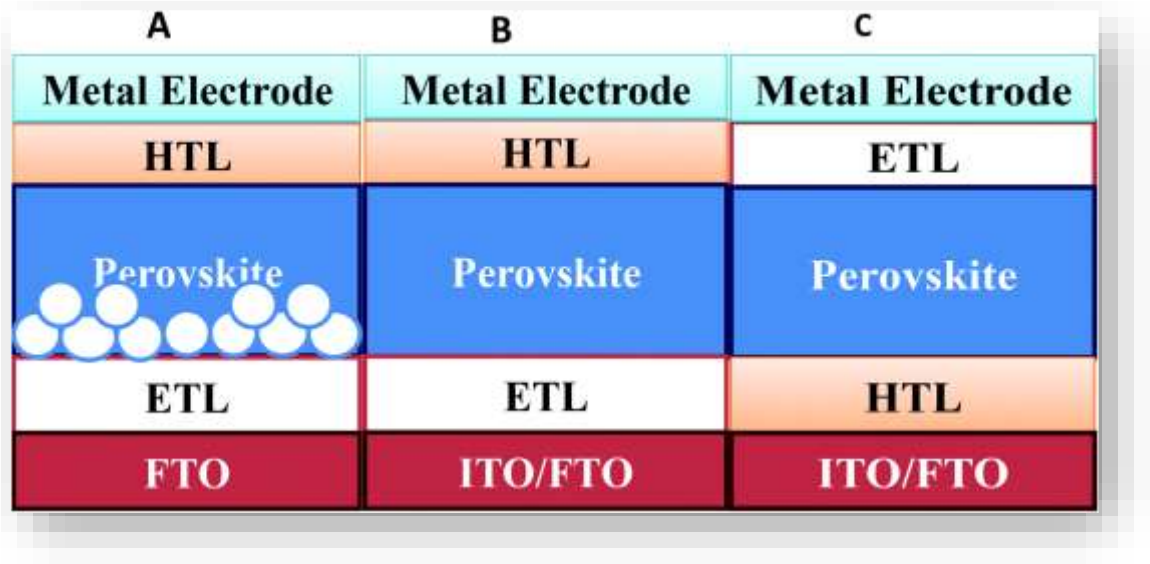

Figure I.12: Generic structure conventional mesoporous (A), and n-i-p (B) and inverted p-i-n (C) planar perovskite solar cell.

I.5.3 Structural properties of perovskite (Active layer)

Perovskite is based on the crystal structure of the mineral calcium titanate (CaTiO3), discovered by German mineralogist Gustav Rose in 1839. It came from a rock sample from the Ural Mountains in Russia, and its physical properties and chemical composition were determined. He named the perovskite in homage to the Russian count Alexeyevich Perovsky, who was also a mineralogist [32].

The perovskite structure can be described by the chemical formula $ABX3$, and is characterized by two cations, A and B, which differ greatly in size, and an anion, represented by "X," which is typically oxygen or a halogen. A is a monovalent cation, which can either be inorganic, such as (Rb+, Cu+), or organic, such as CH3NH3 methylammonium or CH3(NH2)2+ formamidinium. On the other hand, B is a bivalent cation that can be represented by elements such as Cu2+, Ni2, Ge2+, Sn2+, Pb2+, Sr2+, and Ba2+. The perovskite structure is ideally composed of A+ cations located at the corners of a cube, while the anions X occupy the middle of each face, and the B2+ cations occupy the middle of octahedral sites formed by the anions, as illustrated in Figure I.13 [33, 34, 35].

The unique structures and broad range of applications in electrical, mechanical, optical,

magnetic and electronic devices make organic-inorganic halide perovskites a topic of great interest in the field of solar cell research. The combination of organic and inorganic components in hybrid materials allows for the integration of their respective properties, resulting in remarkable characteristics such as high efficiency, light weight, and low-temperature processability. Hybrid perovskites, in particular, exhibit extremely high absorption coefficients [36, 37]. For instance, $CH_3NH_3BX_3$, also known as MA+ (where B is Pb or Sn, and X is Cl, Br, or I), was utilized in 2009 as the first functional hybrid perovskite solar cell. The remarkable efficiency of approximately 3.8% [38] exhibited by methylamonium lead iodide ($CH_3NH_3PbI_3$) confirms that it behaves primarily as an intrinsic semiconductor, capable of transporting both electrons and holes [39].

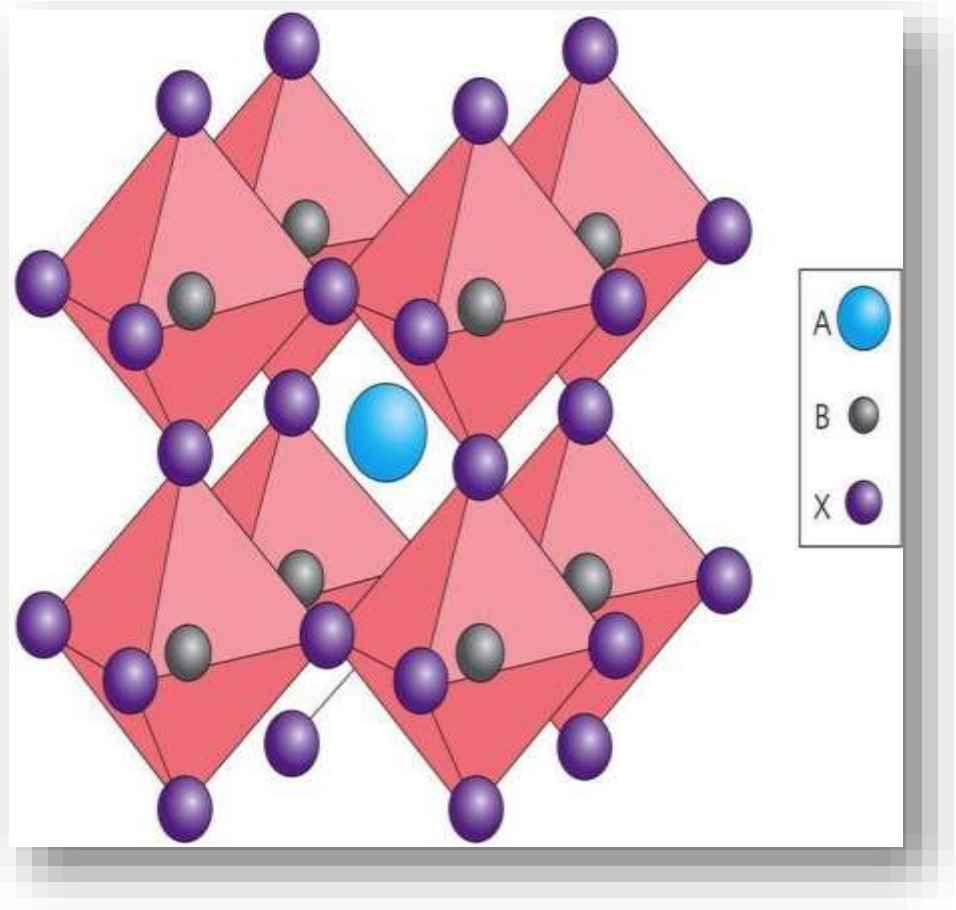

Figure I.13: the general formula of the perovskite structure ABX_3 on right.

I.5.4 Optoelectronic properties of perovskite materials

The exceptional optoelectronic characteristics of perovskite materials that can be solution-processed has generated significant interest within the scientific community. These properties have been extensively researched in recent years, with the main focus on improving the efficiency of perovskite solar cells and gaining a deeper comprehension of the material's electrical and optical properties. These properties include the ability to adjust the band gaps for optimal light absorption, high absorption coefficients, lengthy carrier diffusion lengths, and superior carrier mobility. These efforts have been documented in numerous studies and publications during the past several years [36, 37].

The bandgap parameter plays a crucial role in the effectiveness of photovoltaic materials. This is because, according to the Shockley-Queisser limit, the ultimate potential efficiency is contingent upon the bandgap of the material. CH3NH3PbI3 functions as an intrinsic semiconductor, boasting a band gap of 1.55 electron volts [36, 37]. Consequently, it has an absorption onset that is in close proximity to 800 nanometers, with a corresponding absorption coefficient of roughly 105-106 cm^{-1}. This allows for the visible spectrum to be strongly absorbed. As a result, thin absorbing films that are around 300-600 nanometers in size are usually deemed satisfactory for solar cells, as they are able to effectively absorb light while also promoting good charge collection [36, 37].

At room temperature, the excitons that are induced by the photograph rapidly disintegrate into free charge carriers due to their low binding energy, which is approximately 50 meV. These carriers have a minute effective mass, thus producing a mobility of 24±7 cm^2/Vs for electrons and 105±35 cm^2/V.s for holes. The recombination of these carriers occurs on a timescale of hundreds of nanoseconds, thus leading to long carrier diffusion lengths between 100 nm and 1 µm [36, 37]. Another attractive property of perovskites is the ability to tune their bandgap by changing the combination of cation and anion components in the crystal structure. This is done to enable colored solar cells for various architectural applications and to increase the coverage of the visible spectrum of the sun [39].

I.5.6 Deposition methods of perovskite films

Various techniques and methods have been developed to produce higher quality perovskite films. Based on the same principle, the combination of organic and inorganic components.

One-step deposition or spin coating is the most commonly used deposition method because it is easier to operate and low cost. Perovskite is in commonly used solutions: Typically,

precursor solutions are dissolved in gamma-butyrolactone (GBL), N, prepared in N-dimethylformamide (DMF), and dimethyl sulfoxide (DMSO) [40, 41] or a combination of two or all three solvents followed by rotation (Figure I.14.a).

The two-step deposition method was developed for depositing perovskite thin films at low temperatures as a second method to improve one-step deposition, which resulted in poor and uneven surface coverage. The two-step deposition process does not require complete preparation of the precursors, but separates the coating from the PbI2 and MAI. First, the metal halide precursor PbI2 is used to deposit the film, mainly using the spin coating process, and then the substrate coated with the film is immersed in the second precursor solution MAI, and the final perovskite film is formed after proper baking. Although the steps become more complex [3, 40, 41, 42, 43] (Figure I.14.b).

Other types of modified deposition processes for depositing perovskite films have also been developed, including the vapor-assisted solution process, which can be viewed as an improved, process-based two-step process for depositing perovskite films. MAI was incorporated on a PbI2 seed layer deposited by spin-coating using a vapor-phase deposition technique, and MAI vapor was formed at 150 °C without problems of incomplete **conversion** and limited solubility (Figure I.14.d). Perovskite films with complete surface coverage, low surface roughness, and grain sizes up to microns were obtained [40, 41, 42, 43]. Thanks to this dual-source vapor deposition method of simultaneously depositing organic and inorganic precursors, perovskite films with excellent uniformity were produced, which subsequently significantly enhanced the performance of solar cells [40, 41] (Figure I.14.c).

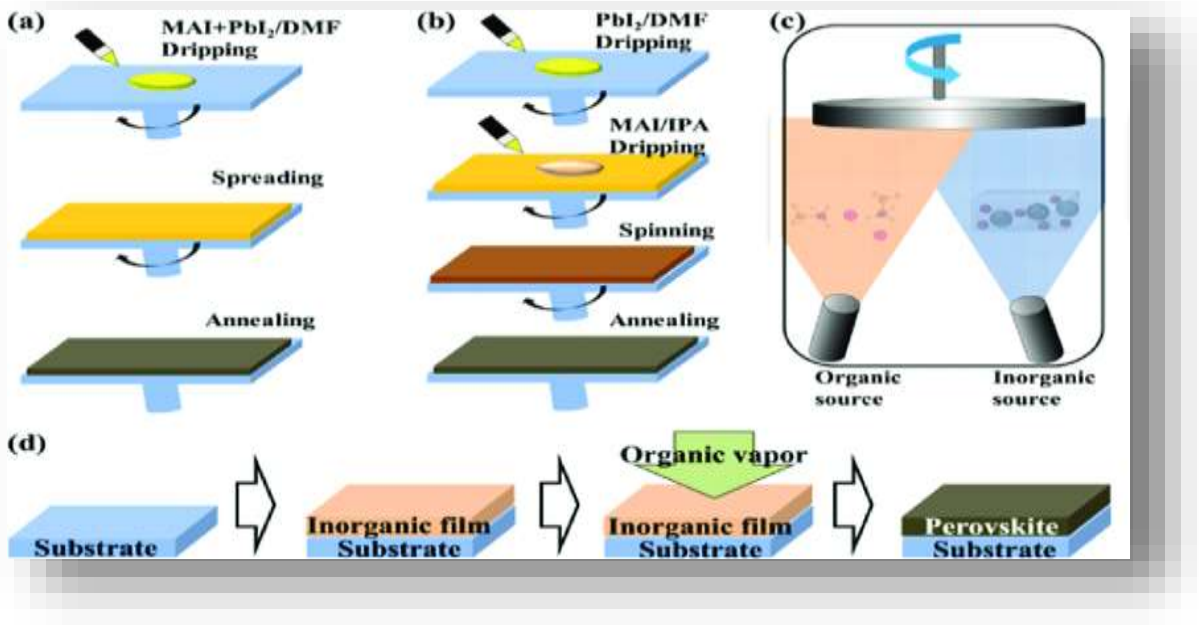

Figure I.14: Fabrication methods of a perovskite films: (a) one-step spin-coating method; (b) twostep deposition method; (c) dual-source vapor deposition; and (d) vapor-assisted solution process.

Chapter II

CuSCN inorganic hole transport material

Chapter II: CuSCN inorganic hole transport material

II.1 Introduction

Optically transparent semiconductors, which can be solution-processed at low temperatures over large area substrates, are in great demand within the electronics industry. Hole-transporting (p-type) materials that fit this description can be utilized as hole injection, extraction and transport inter layers in various optoelectronic devices and systems. They are at present incorporated into numerous optoelectronic devices including OLEDs [44, 45], organic photovoltaics (OPV) [43], and hybrid organic-inorganic photovoltaic cells [45]. Thin-film transistors (TFTs) based on materials with the aforementioned properties are also required for large-area microelectronics applications such driving back planes for optical displays [45, 46, 47]. In most cases, the hole mobilities of transparent intrinsic semiconductors (e.g. metal oxides) are inherently lower than the corresponding electron mobilities [46]. Such low hole mobilities primarily arise from the spatial overlap of electronic wave functions contributing to the hole-transporting valence band being smaller and the bands beings less disperse. Furthermore, most intrinsic wide-bandgap semiconductors do not have an electronic or physical structure that facilitates successful acceptor doping in order to generate a surplus of mobile holes as the majority carriers.

The objective of this chapter is to know the role and Ideal characteristics of HTMs materials exactly the Copper (I) thiocyanate (CuSCN) moreover to define the CuSCN inorganic hole transport material and the Architecture of CuSCN -base de perovskite solar cell.

II.2 Inorganic Hole transport material

Inorganic materials are considered as promising materials for HTM layers due to their properties Favorable properties such as high hole mobility, low production cost, better chemistry Stable and suitable price. CuSCN, CuI, Cu2O, CuO, NiO, MoOx, CZTS and carbon materials (including graphene and Carbon nanotubes (CNTs) are used as inorganic HTMs in perovskite solar cells [47]. Among the suggested materials, copper thiocyanate (CuSCN) is suitable. OK Alignment between HOMO levels of CuSCN and CH3NH3PbI3, and mobility plays a crucial role between materials with nearly similar ribbon alignment properties [47]. Kesterite-structured Cu2ZnSnS4 (CZTS) nanoparticles with narrow bandgap (1.5 eV) and large pores Fluidity (6-30 $cm^2V^{-1}s^{-1}$), high absorption coefficient, rich in elemental composition than

the earth [47]. Therefore, this material can serve as an inorganic HTM for organo lead halide PSCs.

II.3 Background on CuSCN

CuSCN is a single ionized copper molecular metal pseudo halide (a polyatomic group containing a pseudo halide anion, such as thiocyanate) that behaves chemically like a halide ion [48, 49] and is an intrinsic semiconductor that exhibits p-type conductivity. Cuprous thiocyanate material can exist in two forms: alpha phase and beta phase. The α phase has an orthorhombic lattice, and the β phase is more stable and can easily exist in a hexagonal or rhombohedral structure (Figure II.1). The structure of β-CuSCN has SCN ionic layers separating Cu atomic planes and three-dimensionally connected strong Cu-S bonds. This structure is more stable.

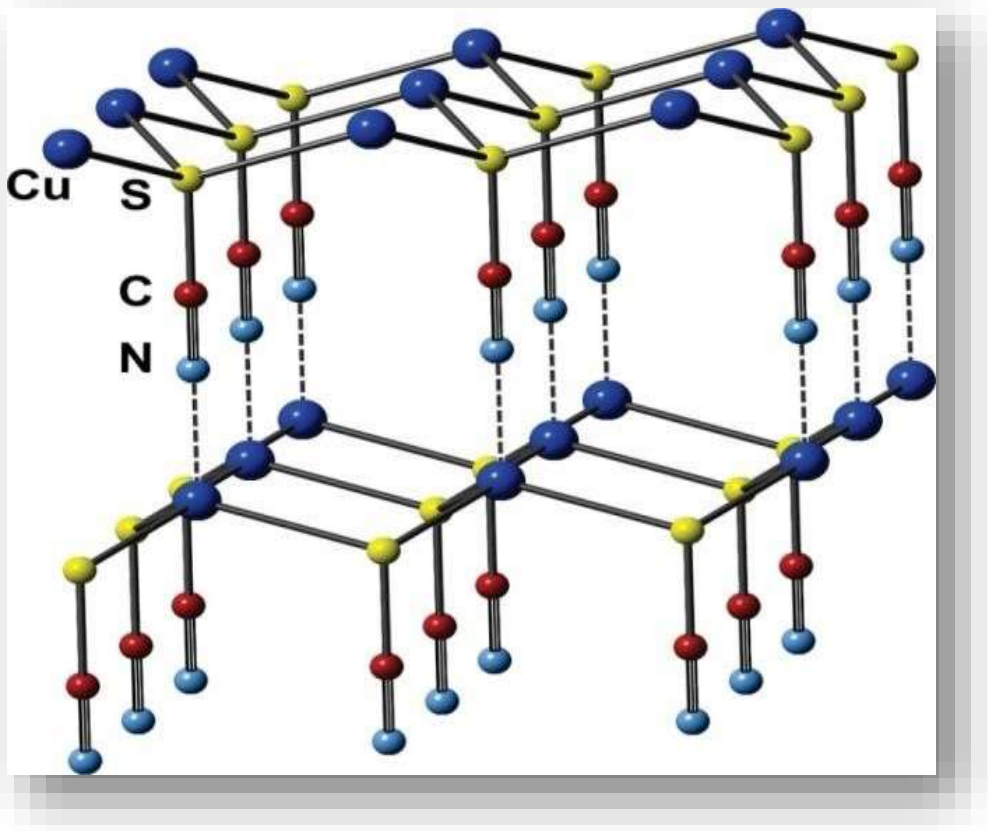

Figure II.1: Structure of β-CuSCN.

Chapter II: CuSCN inorganic hole transport material

II.3.1 Copper (I) thiocyanate (CuSCN)

CuSCN is a molecular, metal pseudo halide of singly-ionized copper, the properties of which have been studied since the first half of the twentieth century [48].Pseudo halide are polytomic groups that incorporate a pseud halogen anion such as thiocyanate and are described as such because they behave similarly to halide ions in chemical reactions [49]. When CuSCN is dissolved, the solvent molecules can from complexes with $CU^{+}$and thereby break or weaken the ionic bond to SCN^{-}. It is a molecular metal pseudo-halide of singly ionized copper behaves like halide ions chemical reactions [48]. CuSCN is an inexpensive and commercially available material, supplied to laboratories by large-scale international distributors. Readers should note that another copper thiocyanate compound also exists: Cu (SCN) 2. While the latter was the subject of several early experiments on pseudo halides. As source of clean energy solar cells have great potential to dominate future energy markets solar energy currently accounts for a very small percentage of electricity used globally but solar cells can be integrated with relative ease into infrastructure and commercial products [49].

Copper (I) thiocyante (CuSCN) hole-transport layers processet from aqueous precurs or solution and their application in thin-film transistor and highly efficient organic and organ metal halide perovskite solar cells: dissolution of copper thiocyanate (CuSCN) in an aqueous ammonia enables processing of superior quality hole transporting layers at low temperature in ambient air [49].

II.3.2 Properties of CuSCN

II.3.2.1 Electronic Properties of CuSCN

Although CuSCN has only recently emerged as a potential material for hole transportation in optoelectronic applications, there have been few theoretical studies published on its electronic properties. The density functional theory (DFT) calculation is predominantly used in these studies to shed light on the electronic configuration of the most commonly used form of CuSCN. The hexagonal β-CuSCN (shown in Figure II.2) is typically observed in experiments [50, 51, 52].

The results of the valence band (VB) and conduction band (CB) structures of different studies are consistent with each other, and two important features near the band edge are (1) strong Cu 3d features with some hybridized states of S 3p near the (VB) edge and (2) Antibonding

π*features associated with cyanide moieties near the (CB) edge. These properties lead to excellent hole transport and a predicted large indirect bandgap, both of which lead to the predominantly p-type character in the visible region and extremely high transparency.

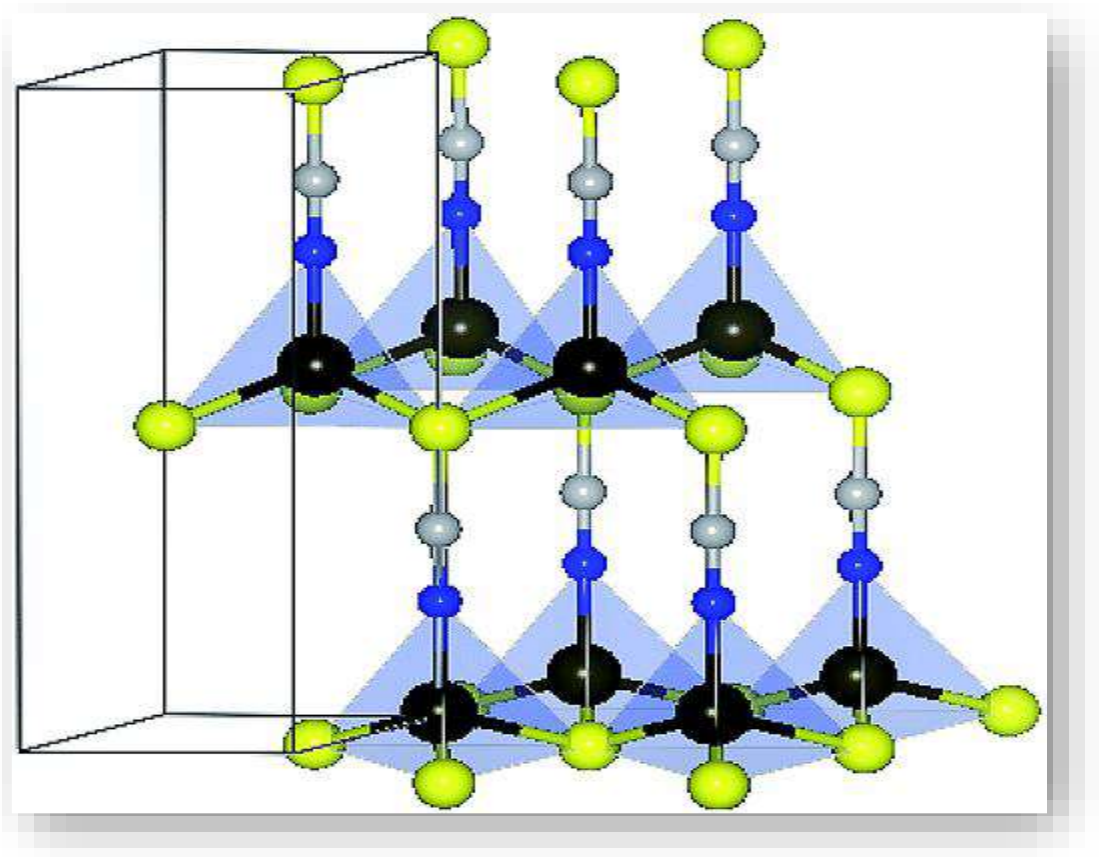

Figure II.2: Crystal structure of hexagonal β-CuSCN. Atoms are color-coded as dark brown for Cu, yellow for S, grey for C, and blue for N.

II.3.2.2 Electronic Band Structure of CuSCN

Figure II.3 presents the band structure. The Various DFT calculations [50, 51, 52] produced qualitatively consistent results for the band structure of hexagonal β-CuSCN (one set of results [50] is shown in (Figure II.3) while the Brillouin zone of the hexagonal lattice [51] is shown in (Figure II.3) (see Figure II.4). All agree that the indirect bandgap has a VB maximum (VBM) at the Γ point and CB minimum (CBM) at the Kpoint (Figure II.3 and Figure II.4). A DFT method using the generalized gradient approximation (GGA), which is known to underestimate

the bandgap, revealed a relatively small bandgap of about 2ev. However, by using the heyd-Scuderia-Ernzerhof (HSE) hybrid function to perform DFT calculation.

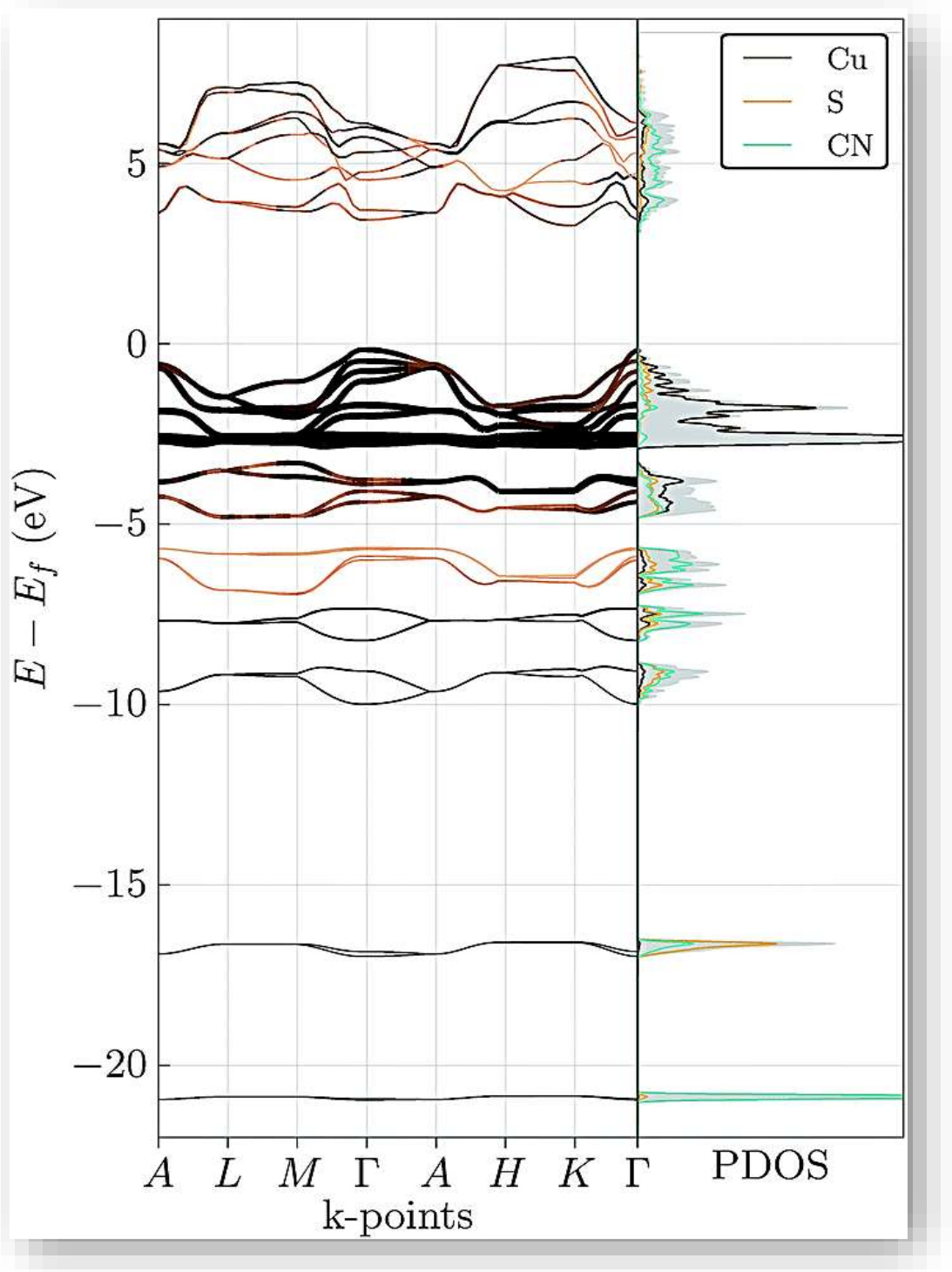

Figure II.3: Electronic band structure of hexagonal β- CuSCN calculated by DFT with HSE hybrid functional.

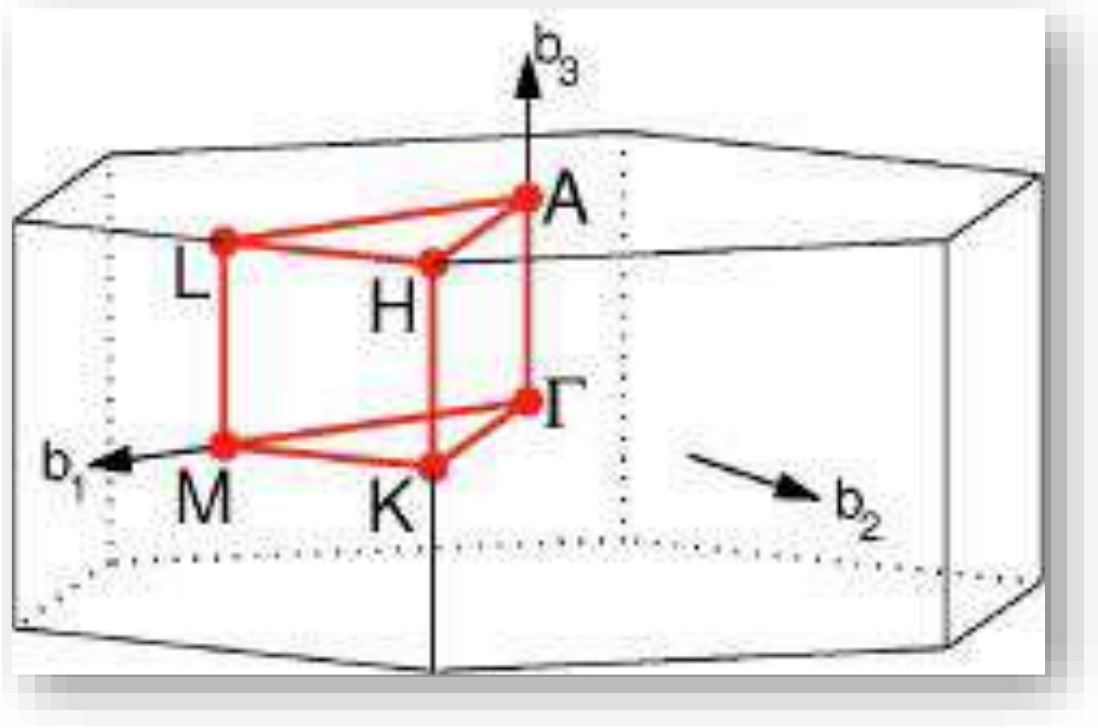

Figure II.4: Brillouin zone of a hexagonal lattice showing the high-symmetry path typicallyused in the electronic band structure calculations.

II.3.2.3 Density of States in CuSCN

Figure II.5 shows the overall density of states (DOS) and partial density of state (PDOS) of hexagonal β- CuSCN in more detail. The VB peak from the VB edge (E= 0 eV) to about -2.5 eV is dominated by Cu 3d states with some contribution from S 3p states. There are four subbands from -3.5 to -10 eV. The first three subbands are centred at -4, -6 and -7 eV, mainly from the p-states of S, C and N, and may be related to the π bonds within the –SCN unit. In addition to the S 3p and N 2p states, the highest of these three sub bands (centred at - 4 eV) also comes from the Cu 3d state, which may also reflect the bonding between Cu and the coordinated S and N- The featured state is off. The last of the four sub bands, at about -9 eV, is dominated by S 3p and C 2p states, suggesting a SAC bond. The photoemission spectra of CuSCN near the VBM in this energy range are in qualitative agreement with the calculated DOS, There are also two deeper sub bands in VB that mainly contain the states of S, C and

N. The subband around -16 eV may be related to the S-C bond, while the subband centred at -19 eV may come from the σ bond of the cyanide moiety. with increasing binding energy, the VB features of hexagonal β- CuSCN includes bonding between Cu 3d states and some hybridization of S 3p states, coordination between Cu 3d states and S 3p and N 2p states, and π bond and σ-bonds in the the-SCN unit, respectively [51].

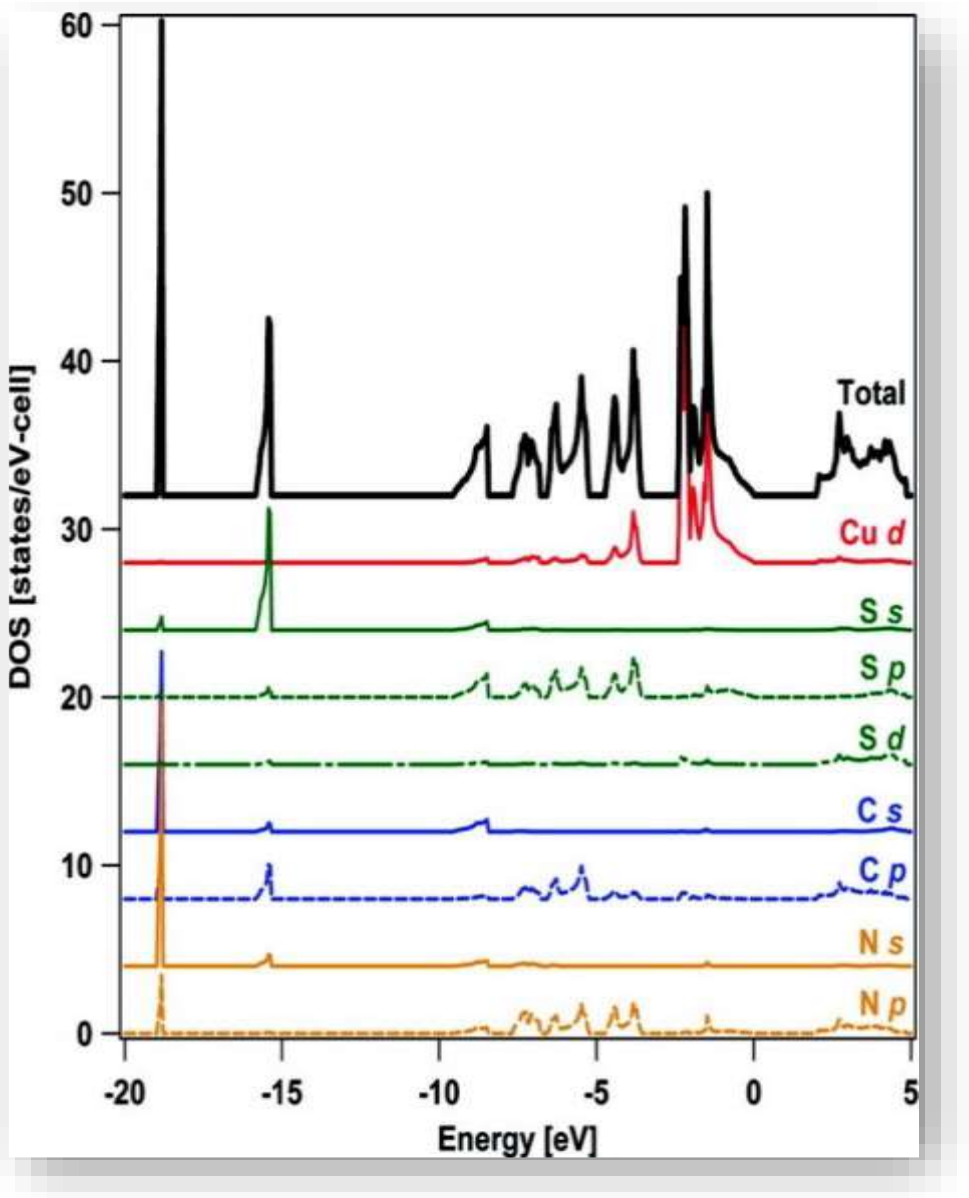

Figure II.5: Calculated total and partial densities of states of hexagonal β-CuSCN showing the contributions from different states of the constituents of CuSCN.

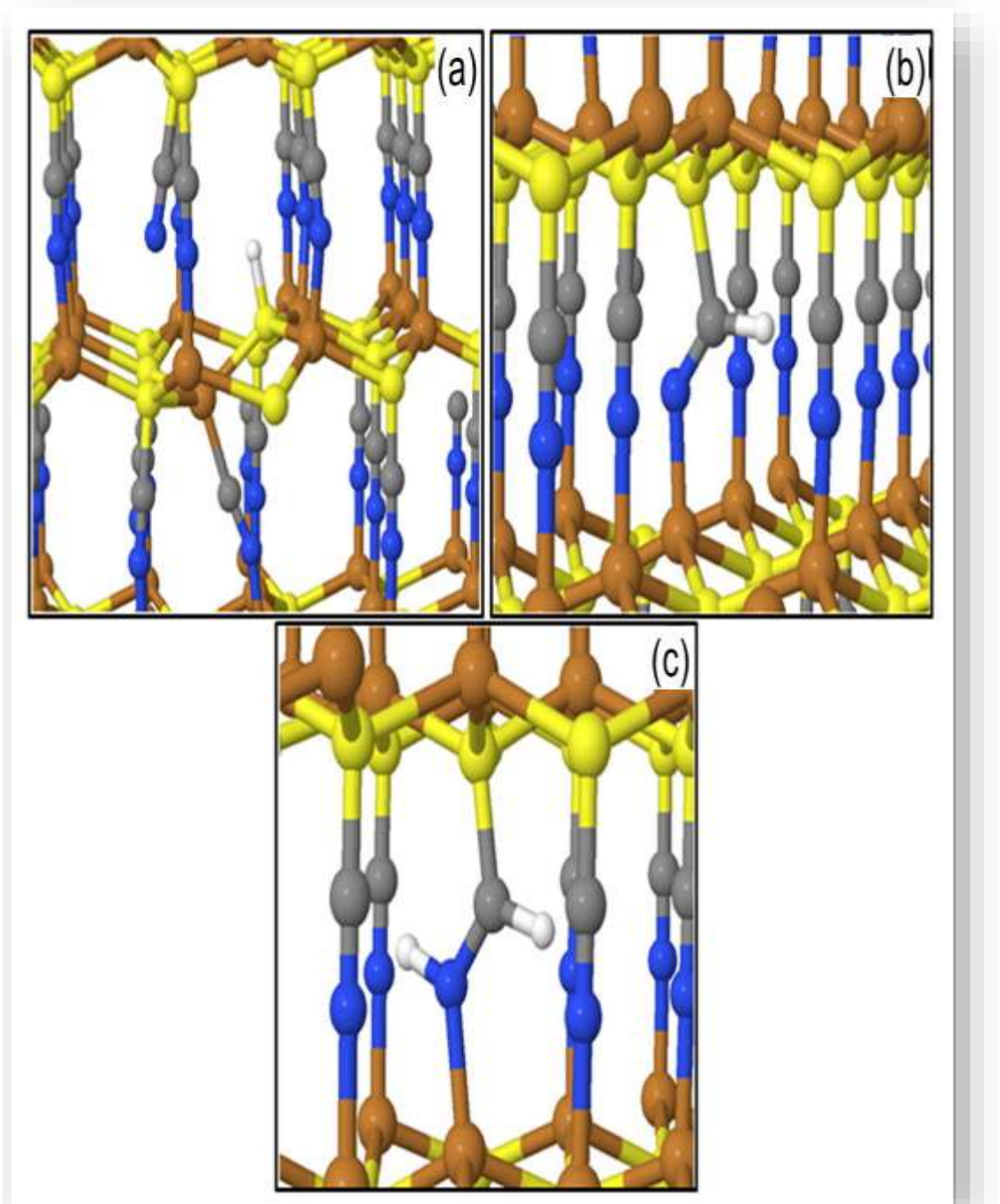

Figure II.6: Single H impurity in hexagonal β-CuSCN forming (a) S–H bond and (b) C–H bond. (c) Two H impurities hydrogenating the cyanide portion. Atoms are color-coded as brown for Cu, yellow for S, grey for C, and blue for N.

II.3.2.4 Structural properties of CuSCN

Depending on the preparation procedure, CuSCN precipitated from solution can exist in two forms, its α-and β-phases, which specify structural parameters such as bond angle [50].

The α-phase has an orthorhombic crystal lattice, while the β-phase can be a hexagonal or rhombohedral structure [51]. Although some studies suggest that polymorphic systems containing both phases may be observed, thin films commonly exhibit the β-phase [51]. CuSCN is an intrinsic semiconductor, which can exhibit p-type conductivity if the solid is formed in a solution where the concentration of thiocyanate ions is higher than that of copper ions.This condition creates a stoichiometric deficiency of copper atoms in the solid, and the hole-transporting character in p-CuSCN is attributed to copper vacancies in the crystal lattice, with acceptor impurity levels generated close to the valence band maximum. Furthermore, the copper defect structure contributes to its optical transparency, because the removal of copper atoms from the perfect crystal lattice broadens the optical angle [51]. Conversely, a stoichiometric axcess of copper atoms has the opposite effect and facilitates greater n-type conductivity. Moreover, CuSCN demonstrates excellent thermal stability since the decomposition of the material into copper In particular, hexagonal copper (I) thiocyanate, the so-called β-CuSCN phase, has been considered to be a promising hole conductor because of its excellent hole mobility, high chemical stability and optical transparency in the entire visible-light range with the band gap of 3.5 eV [52].

Over the last few years, significant progress has been made towards using CuSCN as HTM for the PSC devices, for example, Ito and coworkers developed a suitable doctor-blade method to coat the CuSCN layer over the perovskite layer and improved the photovoltaic conversion efficiency (PCE) of the CuSCN-based PSCs up to 12.3% [52].

CuSCN exists in α-and β-phase, with the structures given in Figure II.7. It has been reported that β-phase is more stable and is easily accessible. The α-and β-phase can be classified as orthorhombic and hexagonal or rhombohedral structures, respectively [53].

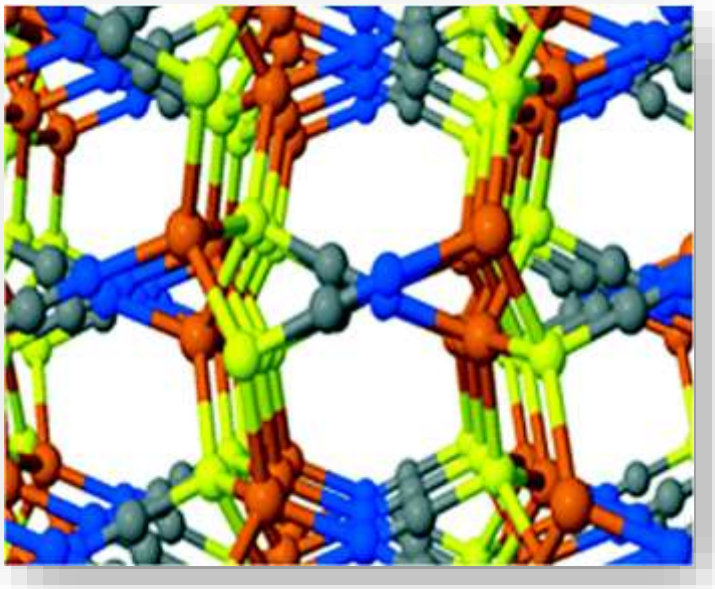

(a)

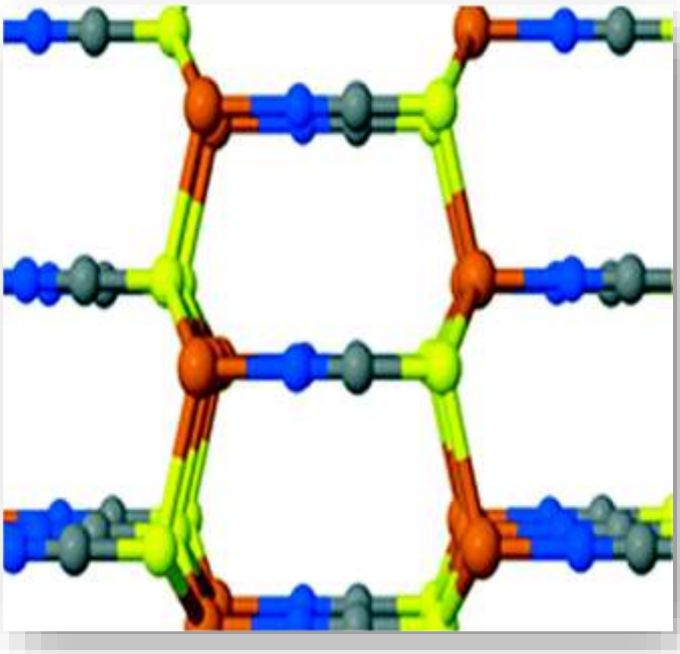

(b)

Figure II.7: bulk three-dimensional phases of CuSCN : (a) α-phase(orthorhombic) ; (b) β-phase (hexagonal) where brown sphere =Cu ; yellow sphere = S ; gray sphere =C ; and blue sphere = N.

II.3.2.5 Defects in CuSCN

In an earlier study, Tennakone et al [53]. Showed that the conductivity of CuSCN can be tuned to be p-type or n-type by tuning the CuSCN ratio. In particular, the authors obtained two types of CuSCN using chemical bath and electrodeposition methods. According to their chemical method and analysis, the CuSCN ratio of p-type CuSCN is 0.92 to 0.96, while the ratio of n-type CuSCN is between 1.31 and 1.44. Subsequently, it was also shown that doping CuSCN with SCN could improve its p-type conductivity [54] therefore, the extrinsic p-type doping of CuSCN is usually associated with excess SCN or insufficient Cu conditions, and of course, natural defect Cu vacancies (V_{Cu}) are considered to be the main source of the observed excess holes in CuSCN [53, 54].

II.4 Roles and Ideal characteristics of HTM

A huge number of works discussing the integration of inorganic HTMs in PSCs are present in the literature [55]. The reason for this wide interest in similar layers/materials is certainly related to the numerous inorganic compounds that can be applied for this role, their relative ease of processing through versatile technologies (spin coating, spray coating, thermal evaporation, electrospraying), the low cost associated with high-abundant raw materials, and the inherent hydrophobic nature of many of them, which prospects good device stability. In addition, further benefits can be derived by the interfacing of inorganic HTM layers with organic ones, enabling higher levels of control of the hole-extracting properties [56].

Particular mention should be given to bidimensional transition metal dichalcogenides (2D TMDs), whose use in HTMs has been thoroughly discussed in a recent review [53]. Perovskite solar cells have dramatically improved in power conversion efficiency (PCE) since their advent. However, further improvement relies on developing hole-transport materials (HTMs) that are doping-free [19].A highly efficient hole-transporting material (HTM) based on the copolymer of dialkoxybenzen and bithiophene is presented [21].

CuSCN has received significant attention as an HTM in PSC due to the fact that it has higher maximum hole mobility of about 0.1 $cm^2v^{-1}s^{-1}$ which is far larger than of spiro-OMeTAD with a maximum hole mobility of $6\times 10^{-5}cm^2v^{-1}s^{-1}$. Moreover, CuSCN HTM has suitable energy levels as well as affordable and simplified synthesis routes as compared to sprio-OMeTAD which makes it ideal for large-scale application[22].

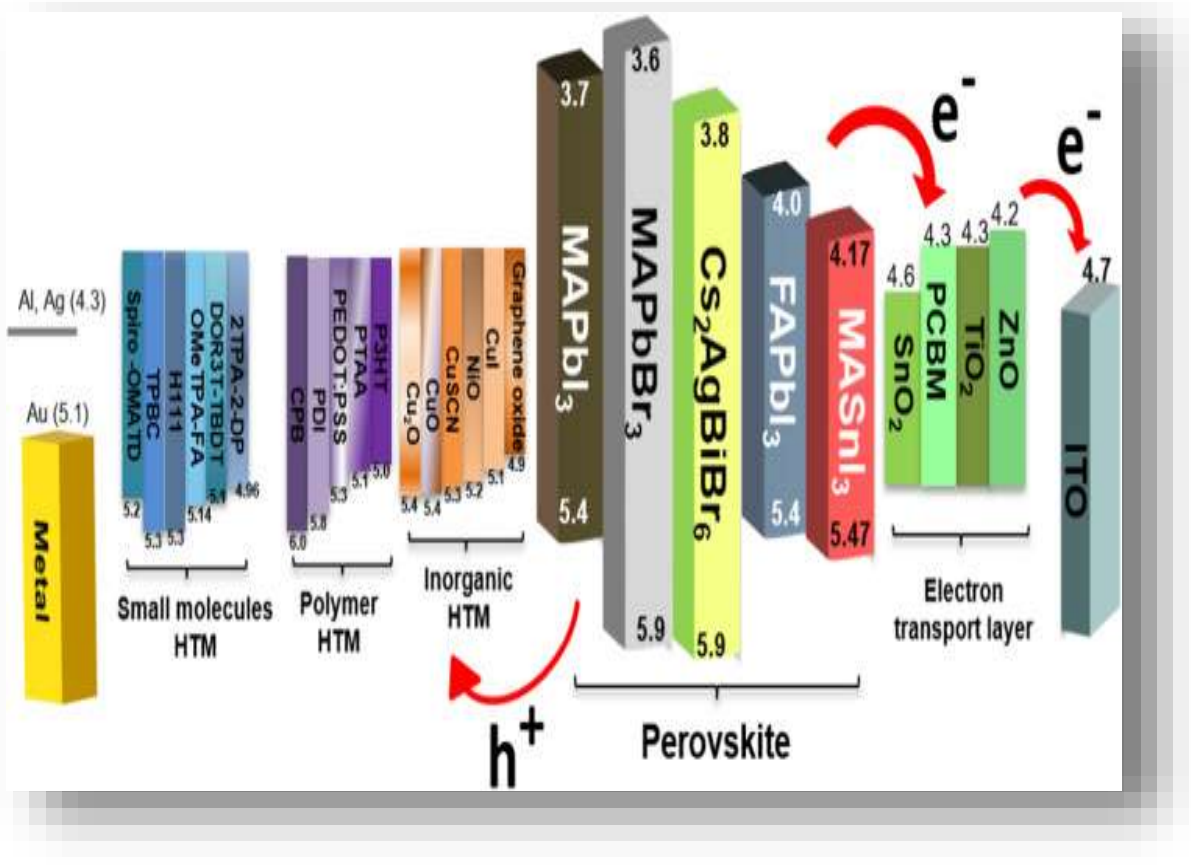

Figure II.8: Advances in hole transport materials engineering for stable and efficiency perovskite solar cells.

II.5 Hole transport in CuSCN

Although the stoichiometric CuSCN is known to be an inherently Hole transport semiconductor, extrinsic p-type conductivity was observed at room temperature and Attributed to the formation of nearby acceptor impurity levels The valence band maximum due to the presence of copper Voids in the lattice [57]. Last field effect Hole mobility values as high as 0.1 cm2 V^{-1} s^{-1} have been reported TFT based on solution-processed nanocrystalline CuSCN Movies [58]. Turns out the device is ready and tested Exhibits intrinsic hole transport properties in an inert atmosphere but there is a significant p-type doping effect observed when the transistor was exposed to air for a period of time sky. In addition to the external doping effect, hole transport also occurs CuSCN is also known to perform strongly Depending on fabrication conditions and device geometry, Electrode

Contact Resistance and Dielectrics/Semiconductors interface trap density. But that the underlying physical mechanism remains to be studied and requires further work.

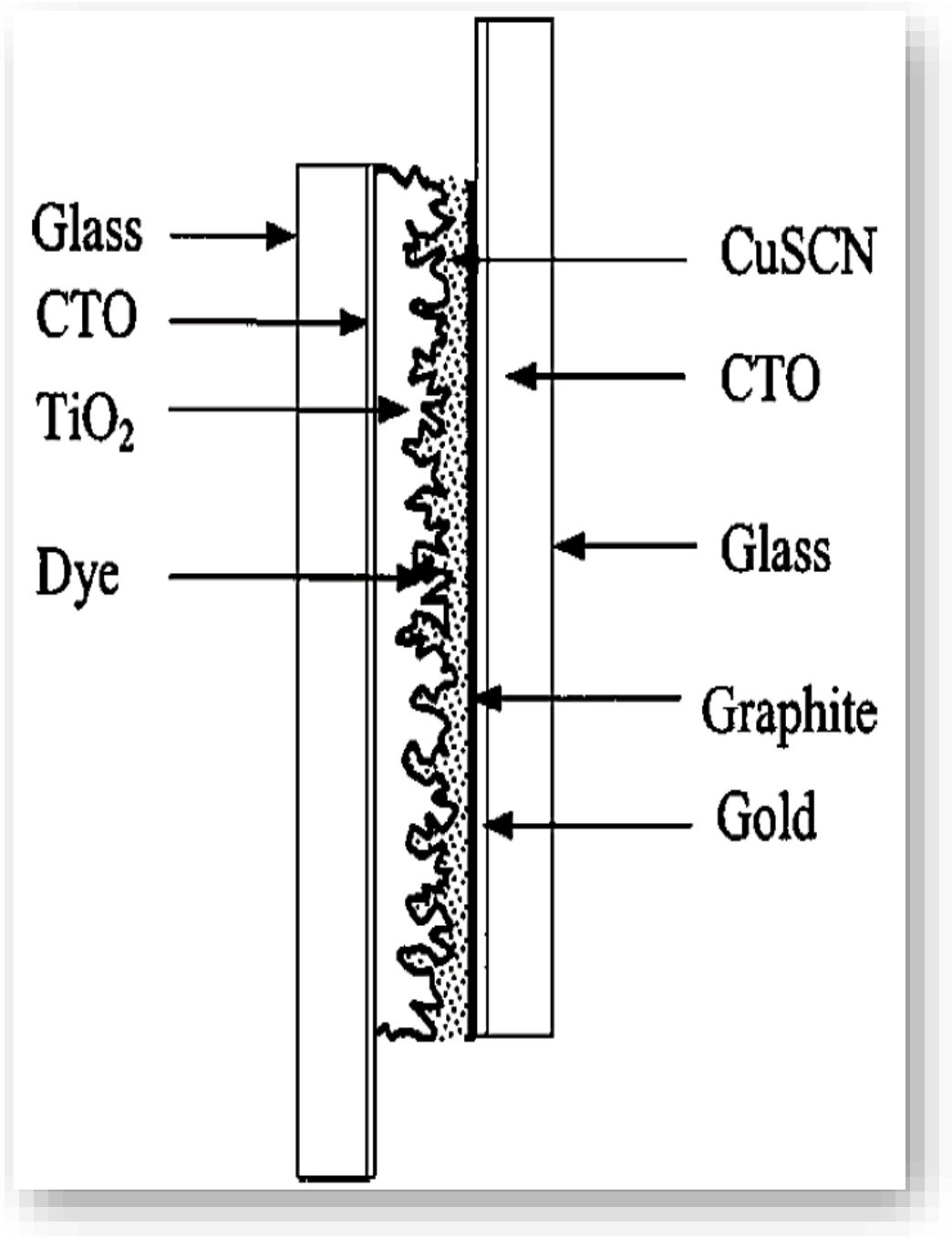

Figure II.9: Schematic of a dye-sensitized NIR photodetector with n-TiO_2; p-CuSCN.

Chapter II: CuSCN inorganic hole transport material

II.6 Applications of CuSCN

Early studies on CuSCN investigated its photocatalytic properties [59] and its application in the generation of dye-sensitized fabrics Photocurrent [60]. The electronic band structure p-CuSCN limits its applicability as a photocathode Adsorption of Dye Molecules on Semiconductor Surfaces modifying the spectral response of the composite system and increasing sensitivity to light. However, n-type dye-sensitized Titanium dioxide (n-TiO2) shows superior photocatalytic performance characteristics, quickly integrated with nanostructured n-TiO2 films Central component of many dye sensitization systems [61]. p-n heterojunction Contains p-CuSCN and n-TiO2 deposited on a Glass substrate with conductive tin oxide (CTO) coating, Among them, the gold-plated CTO glass substrate is on the opposite side The side acts as the backside contact, After photoexcitation Dye molecules at the semiconductor interface inject holes Valence bands of p-CuSCN and electrons into the conduction band of n-TiO2 to generate a measurable photocurrent. The roughness of the dye-sensitized TiO2 film appears large surface area for light absorption.

The maximum spectral sensitivity of the device can be adjusted by modifying the chemical structure of the dye. However, further research is needed to optimize device responsiveness Response times are competitive with similar NIR detector technologies; Slow Diffusion Transport of Electrons in TiO2 Movies are a particular obstacle. In contrast, the fast response of 4 ns Watching Time in an Ultraviolet (UV) Photodetector Contains CuSCN and Zinc Oxide (ZnO) nanorod Heterojunction [62]. The heterojunction is photosensitive without dye sensitization: As wide bandgap semiconductors, CuSCN and ZnO exhibits high transparency in the visible spectral range, but High-energy photons of ultraviolet frequencies are readily absorbed. The Latest Research on Response Characteristics of Ultraviolet Light CuSCN and ZnO nanorod heterojunctions were also fabricated achieved promising results and further demonstrated their potential Development of a self-sufficient ultraviolet photodetector with fast response the timing of device selectivity can be modulated by controlling the length of ZnO nanorods [63]. Other dye sensitization Systems containing CuSCN discovered in photoelectron chemistry Cells sensitized with CuSCN-based dyes [64] Heterojunctions for photovoltaic cells were soon proposed and implemented by O'Regan and Schwartz [65, 66].

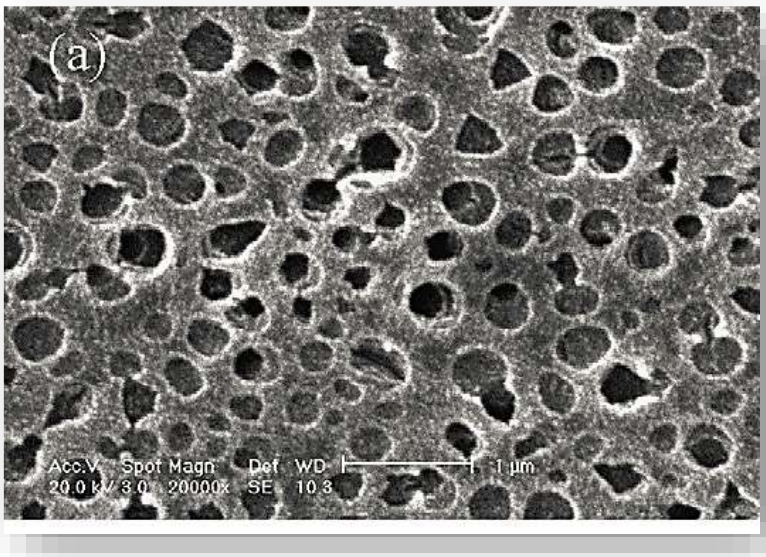

(a)

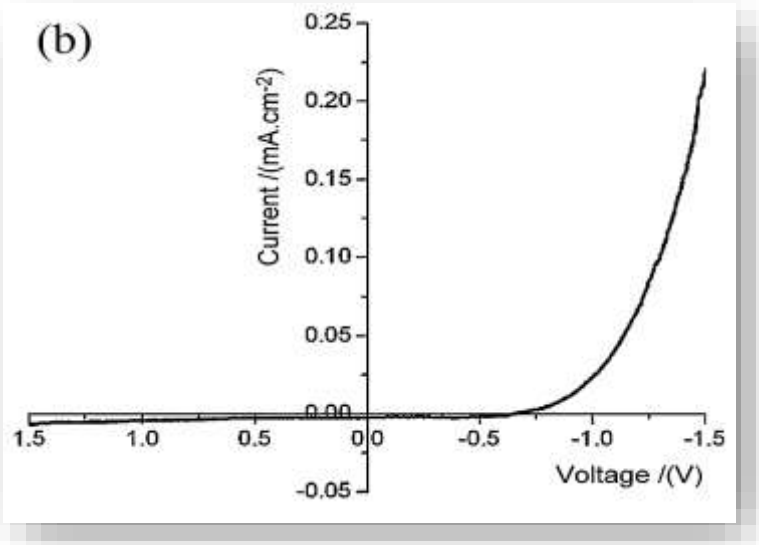

(b)

Figure II.10: (a) An SEM image of the as-prepared porous n-TiO_2 surface into which p-CuSCN is filledto form a heterostructure. (b) Current-voltage characteristic of the corresponding p-n heterojunction.

II.7 (n-i-p) and Inverted (p-i-n) Architecture of CuSCN-Based PSCs

The architecture of PSCs can be categorized into two types based on the layer that is in contact with the transparent conductive substrate: the conventional n-i-p and the inverted p-i-n .In these classifications, n and p refer to materials that transport n-type and p-type charge carriers respectively, while i denotes the perovskite optical absorption layer.

The traditional planar PSCs devices [66, 67, 68, 69] consist of depositing a flat electron transporting layer (ETL) on top of a transparent-conductive oxide (TCO) substrate, typically made of either fluorine-doped tin oxide (FTO) or indium tin oxide (ITO) and used as the cathode. After this, perovskite materials are deposited on top of the ETL by either spin-coating or vacuum evaporation. A flat hole transporting layer (HTL) and metal electrode, such as Au or Ag, are then deposited on top of the perovskite materials , In the case of inverted PSCs [70, 71, 72, 73, 74], a simple exchange of the ETL and HTL positions occurs. On the other hand, mesoporous n-i-p PSCs [75, 76, 77, 78, 79, 80] differ from planar structural PSCs in that they use a compact TiO2 layer on FTO/ITO as the ETL, followed by deposition of a mesoporous TiO2 layer, which acts as both the ETL and structural scaffold. The perovskite film is then formed by depositing the perovskite precursor solution, and the HTL and metal electrode are deposited afterwards.

The primary purpose of the hole transporting materials (HTMs) of a device is to collect and transport after the light harvester injects holes, effectively separating the electrons from the holes, a crucial component of the PSCs. High hole mobility and photochemical stability, suitable solubility in organic solvents and good film-forming ability for processing and device fabrication, suitable highest occupied molecular orbital (HOMO) energy levels for matching with the valence band energy (VBE) of perovskite materials, together with ensuring holes injection and transporting at each interface, and suitable light absorptivity are all necessary for high-performance PSCs [81, 82, 83, 84, 85].

The light-harvesting perovskite layer produces electron-hole pairs when exposed to sunlight [29], [30], and [31]. Then, electrons and holes move from the cathode and anode to the HOMO energy level of the electron transporting materials (ETM) and conduction band of the electron transporting materials, respectively. Finally, a full cycle of the photocurrent is created [32, 32, 33]. The performance of solar cells can be increased by reducing charge recombination by inserting suitable HTMs between the perovskite layer and metal electrode. This will encourage the separation of electrons and holes in the functional layer interface. The stability of HTMs

with consistent thermodynamic and optical characteristics would also aid to increase the stability of PSCs. In humid conditions, perovskite crystal can quickly disintegrate. Therefore, the hydrophobicity of the hole-transporting layer can largely determine the quality of perovskite films. These moisture-repellent hydrophobic hole-transporting layers can ensure that perovskite materials can support crystals with greater grain sizes and fewer grain boundaries. We emphasize the special qualities of HTMs for PSC with outstanding photovoltaic performance in this review [86, 87, 88, 89].

According to the structure and the charge transfer mechanism, the PSCs can be divided into mesoporous and planar configurations as well as normal (n-i-p) and inverted (p-i-n) configurations, as shown in Figure 1. PSCs typically consist of a metal electrode, an electron-transporting layer (ETL), a hole-transporting layer (HTL), a perovskite absorption layer, and a conducting glass such as fluorine tin oxide (FTO) or indium tin oxide (ITO) (Figure II.7).

The electron-hole pair produced by photon absorption on the perovskite absorption layer under sunlight irradiation can be effectively separated at room temperature due to the low exciton binding energy of halide perovskites [86, 87, 88, 89]. The electron-hole pair is then transferred through the ETL and HTL, respectively, to the electrodes. Under actual working conditions, however, PSCs frequently face unavoidable recombination and accumulation of charge carriers, which results in subpar PCEs and stability [85, 86]. Over the past five years, a lot of work has been put into improving PCEs and PSC durability. Several successful approaches have been put forth, including material design for ETL, perovskite layer, and HTL, additive engineering, interface control, solvent engineering, and cell configuration design [86, 87, 88, 89].

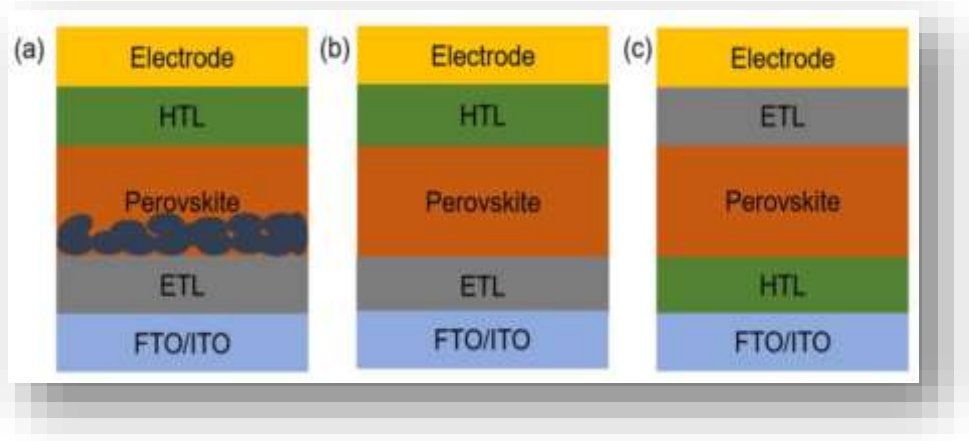

Figure II.11: Schematic diagrams of PSCs with different configurations. (**a**) mesoporous n-i-p structure; (**b**) planar n-i-p structure; (**c**) planar p-i-n structure.

Chapter II: CuSCN inorganic hole transport material

In addition to the poor heat/moisture tolerance and molecular structural instability of contemporary organic HTLs, the instability issue impeding the practical applications of PSCs is also primarily brought on by the inferior stability of organic-inorganic halide perovskites under humid and high-temperature conditions [90, 91, 92, 93]. To transport holes from the perovskite sheet to the metal electrode in PSCs, the HTL is a p-type semiconductor. In order to lessen carrier recombination, HTL also serves as a barrier to prevent the flow of electrons from the perovskite film and to prevent direct contact between the perovskite layer and the electrode. In order to achieve the right energy level alignment, an outstanding HTL material should have high hole extraction/mobility and suitable highest occupied molecular orbit (HOMO)/valence band maximum (VBM) with the HOMO of the perovskite layer [94, 95, 96]. Currently, 2,2′,7,7′-Tetrakis (N,N-di-p-methoxyphenyl-amine)-9,9′-spirobifluorene (Spiro-OMeTAD) is the most widely utilized HTL. It shows acceptable energy level alignment with perovskite layer and the metal electrode. To demonstrate high hole mobility, Spiro-OMeTAD must be treated with lithium salts or 4-tert-butylpyridine; regrettably, this enhances the material's capacity for hygroabsorption, which results in inferior moisture stability [97, 98]. The majority of commonly used organic HTLs for PSCs, such as poly(3,4-ethylenedioxythiophene) polystyrene sulfonate (PEDOT:PSS) and poly(triarylamine) (PTAA), also have this flaw of low heat stability.

In order to substitute their organic counterparts for stable PSCs, inorganic HTLs with excellent inherent structural and thermal stability are seen as very attractive alternatives [99, 100]. The ability of inorganic HTLs to transfer holes has reportedly been significantly improved by the fabrication of nanostructures [101, 102]. Due to their excellent chemical stability, high hole mobility, tunable band gap, and low cost, metal oxide/sulfide-based nanostructures, such as NiOx nanoparticles (NPs), CuIn0.5Ga0.5S2 NPs, Cu2ZnSnS4 NPs, CuSCN NPs, and CuGaO2-CuSCN nanocomposite, have been designed and developed for PSCs. Since the first study in 2014,(Figure II.11) depicts the PCEs progression of PSCs with nanostructured inorganic HTLs. From 9.11% to 21.84%, the PCEs of nanostructured inorganic HTL-based PSCs grew quickly.

Both conventional and inverted PSCs have made extensive use of nanostructured inorganic HTLs. Particularly, nanostructured inorganic HTLs have drawn growing interest in inverted PSCs because of their superior surface morphology and good light transmission capability, both of which are advantageous for the continued deposition of high-quality perovskite films [103].

The PCEs of inorganic HTL-based PSCs with nanostructures, however, are still separated from their organic counterparts it calls for additional research by stressing the requirements for HTLs and the advantages of nano structured inorganic HTLs over their organic counterparts, the most recent developments in the design and fabrication of nano structured inorganic HTLs for PSCs are presented and analyzed in this work. In addition, a number of pertinent methods for improving the performance of inorganic HTLs are discussed, including bilayer HTL building, functional/selective doping, morphological management, nano composite creation, and crystal structure regulation. Finally, prospective research prospects and unresolved issues regarding nanostructured inorganic HTL-based PSCs are also explored. With this review, we hope to offer some new perspectives on the design and manufacture of high-performance, long-lasting inorganic HTL-based PSCs in the future.

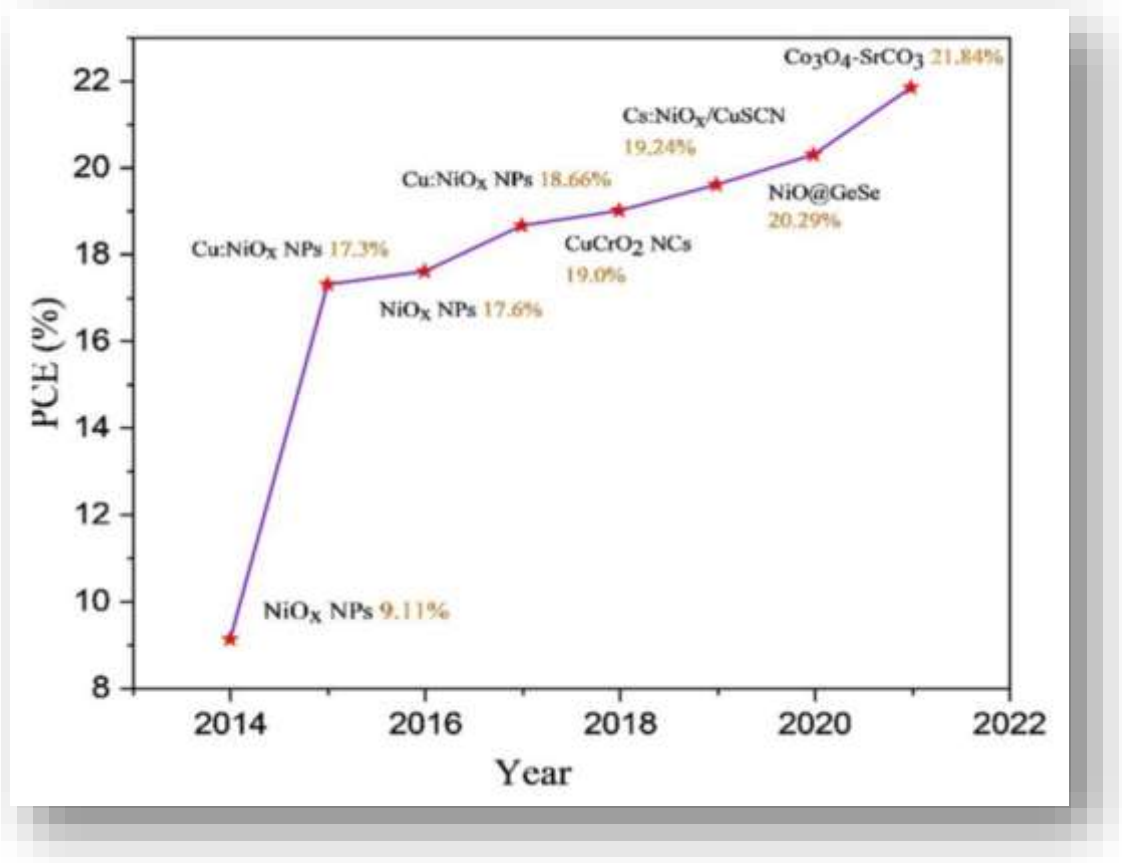

Figure II.12: The PCEs evolution of PSCs with nanostructured inorganic HTLs.

Chapter III

Study of MAPbI3 perovskite solar cell by Silvaco Atlas

Chapter III: Study of MAPbI3 perovskite solar cell by Silvaco-Atlas

III.1 Introduction

Simulation is a technique for studying real dynamical systems by simulating their behavior using a mathematical model of the system implemented on a digital computer [104].

In this work, Numerical simulation is carried out using the SILVACO, for studying the effect of CuSCN on the electrical properties of a perovskite-type solar cell (Jsc, Voc, FF, and efficiency), and studying the doping effect of CuSCN to discover its effects on perovskite solar cell parameters.

III.2 simulation objective

The term simulation refers to the use and development of a model. A model is a theoretical representation of a reality. A problem simulation is an exercise in which a model is developed representing an actual situation. Principal features of simulation:

1) Simulation is a technique oriented toward active participation by the instructor and participants. It also represents an approach or point of entry for providing training in a given situation.

2) It is generally a problem situation and therefore useful in the interdisciplinary development of the teaching-learning process.

3) It is essentially a dynamic technique which is based on changing situations and requires flexibility in thought and response, which must be adapted to whatever circumstances exist at a given time.

A simulator used for a semiconductor component gives the following data as a result [104]:

- Characteristics I-V, C-V, Q-v, G-V……
- 2D curve includes the curve of a quantity such as the potential depending on the vertical distance of a component.
- The 3D curve includes anther parameter for example the vertical distance z.

Chapter III: Study of MAPbI3 perovskite solar cell by Silvaco-Atlas

III.3 Solar cell structure Definition

A solar cell is an electronic device which directly converts sunlight into electricity. Light shining on the solar cell produces both a current and a voltage to generate electric power. This process requires firstly, a material in which the absorption of light raises an electron to a higher energy state, and secondly, the movement of this higher energy electron from the solar cell into external circuit. The electron then dissipates its energy in the external circuit and returns tothe solar cell [105].

Perovskite solar cells (PSCs) have gained a major interest as “third-generation solar cells”.

ABX3 compounds originated from the mineral name of calcium titanate CaTiO3, and belong to a perovskite-type compound. Perovskite materials have suitable material parameters for solar cells such as long electron diffusion length, high optical absorption, small electron and hole effective masses, low processing temperature and strong excitonic transitions. These properties make the organometallic halide perovskites-basedsolar cells achieve comparable efficiencies to the single-crystal silicon and CIGS thin film counterparts.

The studied solar cell is of perovskite type (Figure III.1), the aim of this study of CuSCN material effect on perovskite solar cell [104]. This cell consists of the following layers: transparent conducting oxide, Electron transport layer, Perovskite, Hole transport layer and Electrode.

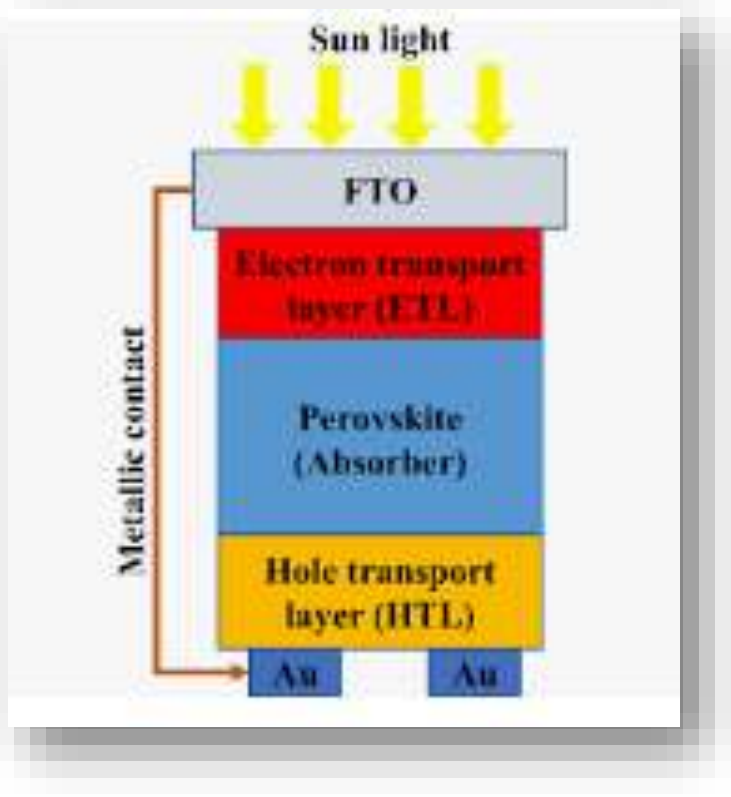

Figure III.1: Perovskite solar cell structure used in this study.

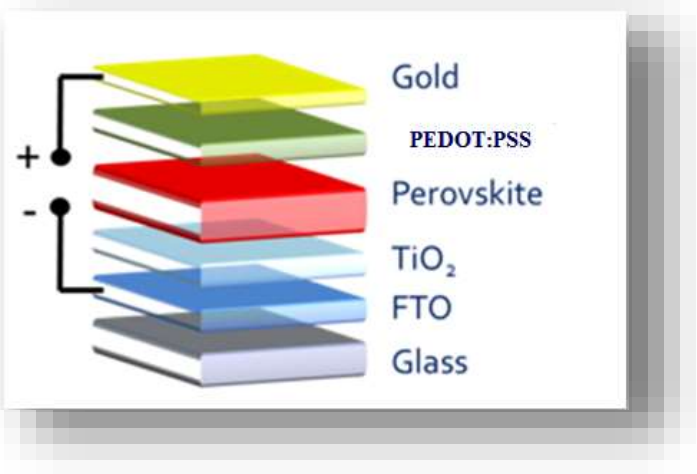

FigureIII.2: Structure for standard perovskite solar cells.

III.4 Silvaco-Atlas

ATLAS is a modular and extensible framework for 1D, 2D and 3D Simulation of semiconductor devices. Implementation is carried out using modern software techniques and Practices that improve reliability, maintainability, and scalability. Use this product The ATLAS Framework meets the device simulation needs of all semiconductor application domains [105].

ATLAS is a physically-based two and three-dimensional device simulator. It predicts the electrical behavior of specified semiconductor structures and provides insight into the internal physical mechanisms associated with device operation [105].

ATLAS produces three types of output files:

- The run-time output.
- The log file.
- The solution file.

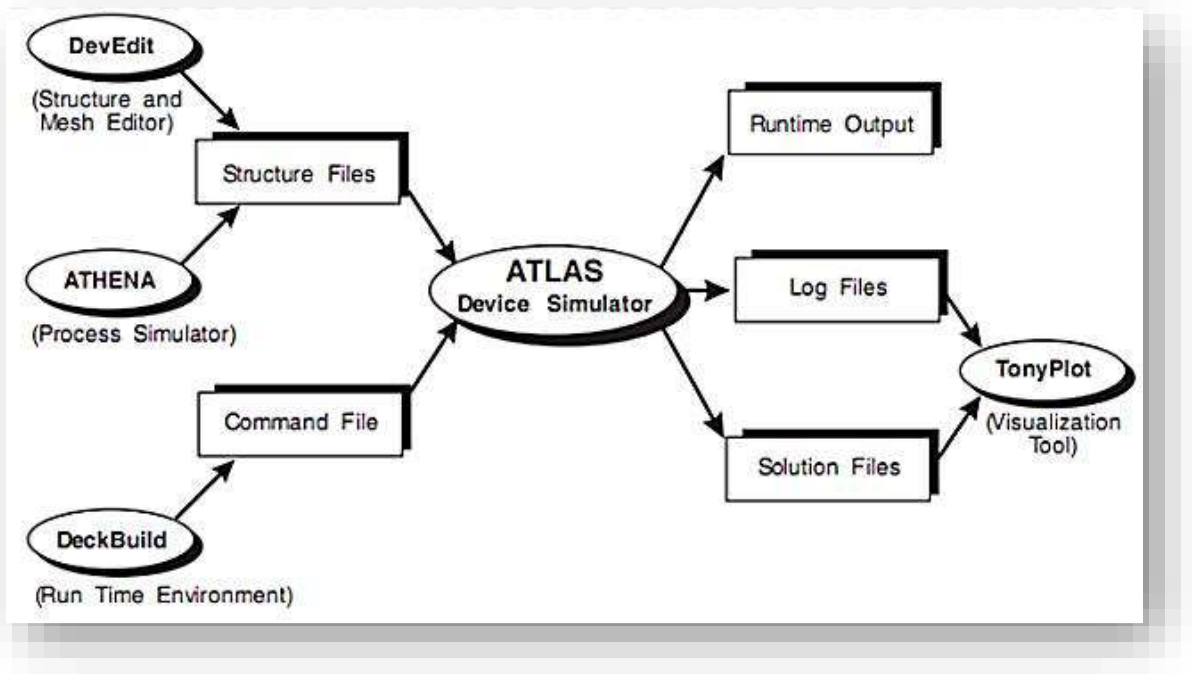

Figure III.3 ATLAS Inputs and outputs.

Chapter III: Study of MAPbI3 perovskite solar cell by Silvaco-Atlas

Since its creation in 1984 by Dr. Ivan Pesic, SILVACO has become the most important semiconductor simulator. SILVACO TCAD is short for Silicon Valley Corporation Technology Computer Aided Design. This is a simulation package of semiconductor processes composed of several physical simulators (ATHENA, ATLAS, MERCURY... etc.) grouped under an environment called DECKBU ILD. Each of them simulates different processes. Due to the large number of modules from SILVACO and their complexity, only the modules used in this work will be presented [105]:

- **DECKBUILD**: is an interactive graphical runtime environment Entry point for developing process and plant simulations. It is considered the main window of SILVACO, where all simulators are located able to control.
- **TONYPLOT:** is a visualization tool that graphically displays the obtained results simulation. It provides scientific visualization capabilities, including XY charts, charts with linear and logarithmic axes Polar, Surface, and Contour plots.

III.4.1 Order of commands in ATLAS

The order of commands in ATLAS includes five groups of instructions which must appear in a specific order as defined in the Table III.1.

Table III.1: ATLAS Command groups with the Primary Statements in each Group.

Group	instructions
Structure specification	Mesh
	REGION
	ELECTRDE
	DOPING
Material models specification	MATERIAL
	MODELS
	CONTACT
	INTERFACE
Numerical method selection	METHODE
Solution specification	LOG
	SOLVE
	LOAD
	SAVE
Results Analysis	EXTRACT
	TONYPLOT

III.4.2 Structural specification

III.4.2.1 The mesh

A mesh refers to a collection of elements whose union defines the peripheral. It is established by overlapping two sets of parallel lines and perpendicular to each other to form an array that has the shape of the device, to generate a mesh in ATLAS, three important pieces of information must be defined [105]:

- The direction of the lines (x.mesh and y.mesh)

- The locations of the main lines (loc)
- The pitch between each line (space) which explains the distance between the linessecondaries in micrometer.

III.4.2.2 Region and materials

After the definition of the mesh, the type of materials and the regions are defined according to the x and y coordinates, using syntax of the form:

Regionnum= <integer> material= <material type><positionsettings>

III.4.2.3 Electrodes

After creating the substrate and semiconductor layers, the next stepis to create contacts on the device. At least one contact must be specified in the script. Due to the metallic nature of the electrodes, a metal must be added to the structure in specific places.The electrodes are defined by the following instruction:

Electrode name =<electrodename><position_parameters>

III.4.2.4 Doping

The doping is defined by the following instruction:

Doping<distribution type><dopant_type><position_parameters><concenter>

III.4.3 Materials

All materials are classified according to their physical properties such as

- ✓ Conductivity (conductors, semi-conductors, insulators).
- ✓ Electron affinity.
- ✓ The energy of the gap.
- ✓ Mobility.
- ✓ Carrier density.
- ✓ Saturation speed.

III.4.4 The models

The physical models implemented in Atlas can be grouped into five groups:

- Mobility Models.
- Recombination Models.
- Carrier statistics Models.
- Impact ionization.
- Tunneling Models and Carrier Injection Models.

III.4.4.1 Models mobility

Electrons and holes are accelerated by the electric fields, but lose momentum as a result of various scattering processes. These scattering mechanisms include lattice vibrations (phonons), impurity ions, other carriers, surfaces, and other material imperfections. A detailed chart of most of the imperfections that cause the carrier to scatter in a semiconductor. Since the effects of all of these microscopic phenomena are lumped into the macroscopic mobilities introduced by the transport equations, these mobilities are therefore functions of the local electric field, lattice temperature, doping concentration, and so on. Mobility modeling is normally divided into: (i) low field behavior, (ii) high field behavior, (iii) bulk semiconductor regions and (iv) inversion layers. The low electric field behavior has carriers almost in equilibrium with the lattice and the mobility has a characteristic low-field value that is commonly denoted by the symbol $\mu_{n0,p0}$ [105]. The value of this mobility is dependent upon phonon and impurity scattering, both of which act to decrease the low field mobility. As already noted, mobility modeling is normally divided into: (1) low- and high-field behavior, and (2) bulk semiconductor regions and inversion layers. Mobility models fall into one three broad categories: physically-based, semi-empirical, and empirical. Physically-based models are those that are obtained from a first-principles calculation, i.e. both the coefficients and the power dependencies appearing in the model are obtained from a fundamental calculation. In practice, physically-based models rarely agree with experimental data since considerable simplifying assumptions are made in order to arrive at a closed form solution. Therefore, to reconcile the model with experimental data, the coefficients appearing in the

physically-based model are allowed to vary from their original values. In this process the power-law dependencies resulting from the first-principles calculation are preserved, and the resulting model is termed as semi-empirical. At the other end of the spectrum are empirically-based models in which the power-law dependencies are also allowed to vary. Table.III.2 below summarizedthe mobility models in SLVACO.When n is the concentration of electrons, p is concentration of holes, T is thelattice temperature, N is the concentration of dopants, E // electric fieldparallel, E $\perp$ the perpendicular electric field.

Table III.2: Mobility models.

Model	**Syntax**	**Notes**
Concentration Dependent	CONMOB	Lookup table valid t 300k for Si and GaAs only. Uses simple power law temperature dependence.
Klaassen Model	Kla	Includes N,T and n dependence. Applies separate mobility to majority and minority carriers. Recommended for bipolar devices
Concentration and TemperatureDependent	ANALYTIC	Caughey-Thomas formula. Tuned for 77-450K
Carrier-Carrier Scattering	CCSMOB	Drokel-Leturq Model Includes n,N and T dependence. Important when carrier concentration is high (e.g,forward bias power devices).
Parallel Electric Field Dependence	FLDMOB	Si and GaAs models. Required to model any type of velocity saturation effect ;
Lombardi (CVT) Model	CVT	Complete model including N, T, E // and E$\perp$effects.Goodfor non-planar devices

III.4.4.2 Recombination Models

Carrier generation is a process where electron-hole pairs are created by exciting an electron from the valence band of the semiconductor to the conduction band, thereby creating a hole in the valence band. Recombination is the reverse process where electrons and holes from the conduction respectively valence band recombine and are annihilated. In semiconductors several different processes exist which lead to generation or recombination, the most important ones are:

- photon transition or optical generation/recombination,
- phonon transition or Shockley-Read-Hall generation/recombination,
- Auger generation/recombination or three particle transitions, and
- Impact ionization.

And we can say that theCarrier generation-recombination is the process by which the material semiconductor attempts to return to equilibrium after disturbance as shown in Table III.3.

Table III.3: Recombination Models.

Model	**Syntax**	**Notes**
Shockley-Read-Hall	SRH	Uses fixed minority carrier lifetimes. Should be in most simulation.
Concentration Dependent	CONSRH	Uses concentration dependent lifetimes. Recommended for Si.
Auger	AUGER	Direct transition of three carriers. Important at high current densities.
Optical	OPTR	Band-band recombination. For direct materials only.
Surface	S.N S.P	Recombination at semiconductor to insulator interfaces. Set on the INTERFACE statement

III.4.4.3 Carrier Statistics Models

The statistics of carriers attempt to better simulate the phenomenon of charge transportation within a device by taking into account the numerous physical phenomena that govern it. As shown in Table III.4.

Table III.4: Carrier Statistics Models.

Model	Syntax	Notes
Boltzmann	BOLTZMANN	Default model
Fermi-Dirac	FERRMI	Reduced carrier concentration in heavily doped region (statistical approach)
Incomplete Ionization	INCOMOLETE	Accounts for dopant freeze-out. Typically, it is used at low temperatures.
Silicon Ionization Model	IONIZ	Accounts for full ionization for heavily doped Si. Use with INCOMPLETE.
Bandgap Narrowing	BGN	Important in heavily doped region. Critical for hipolar gain. Use Klassen Model.

III.4.4.4 Impact Ionization

Ionization by impact is the process by which one charge carrier loses energy while creating additional charge carriers. A sufficiently enough carrier that has been applied to a sufficiently large electrical field may be able to release an electron from the BV and move it to the BC, forming a troubling pair of electrons. There could be an avalanche effect as a result. Some aspects of impact ionization and avalanche breakdown in semiconductors are similar to the

corresponding phenomena in gaseous discharges. Semiconductors may serve as model substances for gaseous plasmas since their ionic charges are practically immobile and therefore the interpretation of experimental data is facilitated. Impact ionization has been achieved both in the bulk of homogeneously doped semiconductors at low temperatures and in p-n junctions at room temperature. The creation of the original charge carrier occurs when a photon is absorbed.as shown in Table III.5.

Table III.5: Impact Ionization.

Model	**Syntax**	**Notes**
Selberherr's Model	IMPACT SELB	Recommended for most cases. Includes temperature dependent parameters.
Grant's Model	IMPACT GRANT	Similar to Selberherr'smodel but with different coefficients.
Crowell-Sze	IMPACT CROWELL	Uses dependence on carrier scattering length.
Toyabe Model	IMPACT TOYABE	Non-local model used with Any IMPACT syntax is accepted.
Concannon	N.CONCAN P.CONCAN	Non-local model developed in flash EEPROM technologies.

III.4.4.5 Tunneling Models and Carrier Injection Models

Hot carrier injection (HCI) is a phenomenon in solid-state electronics in which electrons or "holes" gain enough kinetic energy to overcome the potential barrier needed to breakout of an interface state, as shown in Table III.6.

Table III.6: Tunneling Models and Carrier Injection Models.

Model	**Syntax**	**Notes**
Band-to-Band (standard)	BBT. STD	For direct transitions. Required with very high fields.
Concannon Gate Current Model	N.CONCAN P.CONCAN	Non-local gate model consistent with Concannon substrate current model.
Direct Quantum Tunneling (Electrons)	QTUNN.EL	Quantum tunneling through conduction band barrier due to an insulator.
Direct Quantum Tunneling (Hole)	QTUNN.HO	Quantum tunneling through barrier due to an insulator.
Flowler-Nordheim (holes)	FNHOLES	Same as FNORD for holes.
Klaassen Band-to-Band	BBT.KL	Includes direct and indirect transitions.
Hot Electron Injection	HEI	Models energetic carriers tunneling through insulators. Used for gate current and Flash EEPROM programming
Hot Hole Injection	HHI	HHI means hot hole injection.

III.4.5 Contact

With the "Contact" command, ATLAS is told what to do with the electrodes. A contact electrodes are ohmic standards. If we want to treat the electrodes as With a schottky contact, the corresponding work function must be defined according to the syntax Next:

Contact name=<electrode>work function=<value>

III.4.6 Numerical methods

There are numerous numerical techniques available to compute solutions to semiconductor device problems. The METHOD statements of the input file contain the specified numerical methods, ATLAS will be required to solve up to six equations for various combinations of models. There are three primary solution techniques available for each of the model types: (a) decoupled (GUMMEL), (b) fully coupled (NEWTON), and (c) BLOCK. The GUMMEL method works by solving for each unknown variable individually while holding the other variables constant, repeating this process until a stable solution is reached. The NEWTON method, on the other hand, solves the entire system of unknowns simultaneously. The BLOCK method is a hybrid of the GUMMEL and NEWTON methods, with some equations fully coupled and others decoupled. Specification of the solution method is carried out as follows:

Method<method 1><method 2><method 3>

III.4.7 Solution Specification

In this section, ATLAS is asked to do calculations and find solutions for various equations based on the specified physical and electrical parameters. This is accomplished with the four instructions log, Solve, Output, and save. All simulation results will be recorded in a backup file created by the instruction log. The Solve instruction: calculates data from one or more bias points to DC (direct current) or AC (alternating current). But first, an initial solution simplified must be calculated (which only solves the Poisson equation) to obtain an initial estimate of the final solution. The instruction can be in the form:

Solve init

solve vanode=-10 vstep=0.1 vfinal=10 name=anode

The Save and output statements are used to save the results to a structure file (.str)

III.4.8 Analysis

The analysis section includes two instruction extract and tonyplot.The instruction extract allows one to get and display in the "run-time output" window the value of a result assigned to a particular point, such as:

Additionally, it enables the extraction of data in the form of a courbe for display using Tonyplot.

Extract name="courbe_IV" curve (v."anode", i."anode")

The tonyplot instruction provides graphical data visualization. The end of the program is marked by the instruction Quit.

III.5 Study of J-V characteristics MAPbI3 perovskite solar cell

Perovskite solar cells (PSCs) have been brought into sharp focus in the photovoltaic field due to their excellent performance in recent years. The power conversion efficiency (PCE) has reached to be 25.2% in state-of-the-art PSCs due to the outstanding intrinsic properties of perovskite materials as well as the progressive optimization of each functional layer, especially the active layer and hole transporting layer (HTL).

The perovskite solar cell studied in this work is similar to the first n-i-p solar cell introduced by [106] but with some different. The structure of our perovskite solar cell utilized in this study is shown in (Figure.III.4). It is a one dimensional devise with n-i-p planar heterojunction. The n region is the ETL (TiO_2), the i-region is the perovskite (MAPbI3) layer and the p region is the HTL (PEDOT: PSS). When the cell is subject to light, excitons (bound state of an electron and a hole) are created mainly in the perovskite i layer. According to their diffusion length they can reach the n (p) region. At the n/i interface the exciton is dissociated and the electron moves toward the n layer while the remaining hole migrates towards the player. Similarly, at the i/p interface the exciton is dissociated and the hole moves to the p layer while the remaining electron migrates to the n layer. The dissociation of exitons and the migration of electrons and holes is favored by the electrical field between the n and p layers.

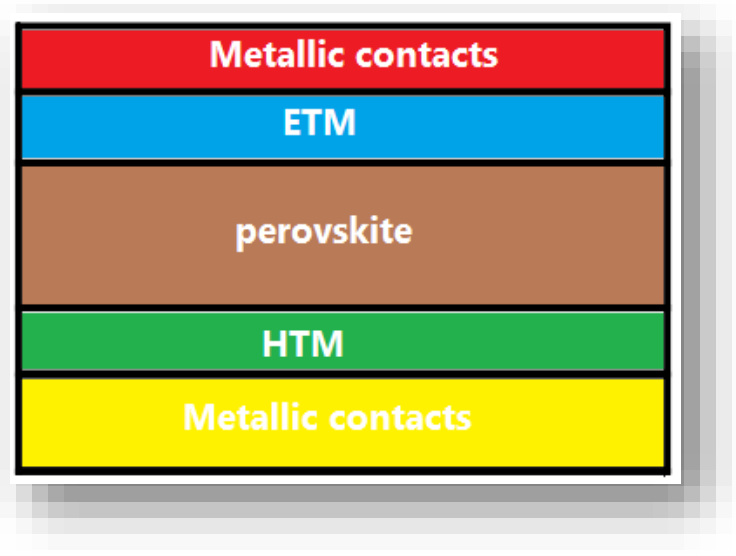

Figure III.4: Device structure of Preliminary (PSC) solar cell.

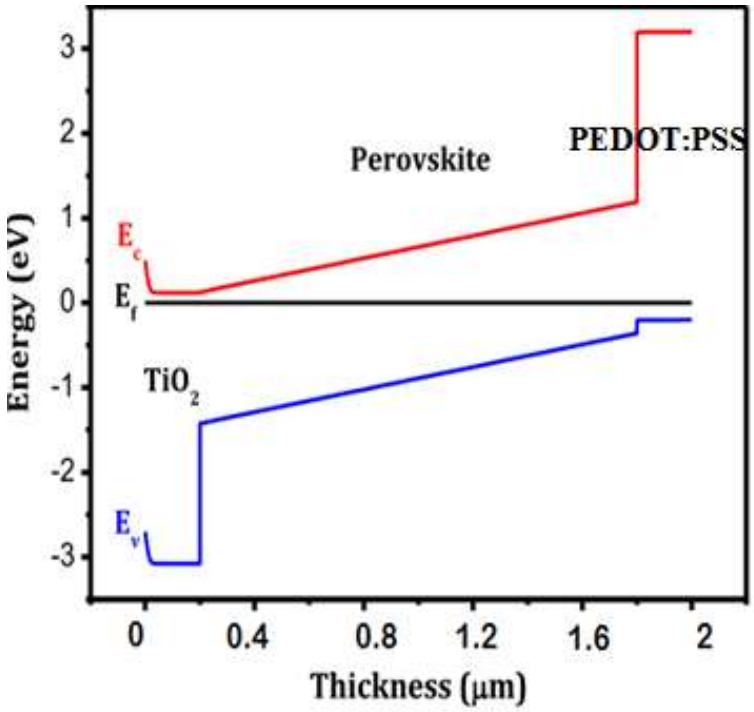

Figure III.5: The band diagram of preliminary (PSC) solar cell.

The input parameters of the structure and the different materials are summarized in Table III.7

Table III.7: Input parameters of MAPbI3 perovskite solar cell.

	ETM(TiO_2)	**Perovskite**	**HTM(PEDOT:PSS)**
d(µm)	0.1	1.9	0.2
E_g(eV)	3.2	1.55	3
χ(eV)	4.1	3.9	2.45
$\boldsymbol{\varepsilon_r}$	9	6.5	9
$\boldsymbol{N_c(cm^{-3})}$	2×10^{18}	2.2×10^{18}	1×10^{19}
$\boldsymbol{N_v(cm^{-3})}$	1×10^{18}	1.8×10^{19}	1×10^{19}
$\boldsymbol{N_d(cm^{-3})}$	2×10^{18}	5.21×10^{9}	0.0
$\boldsymbol{N_a(cm^{-3})}$	1×10^{17}	5.21×10^{9}	2×10^{18}
$\boldsymbol{\mu_n(cm^2/Vs)}$	300	40	1×10^{-3}
$\boldsymbol{\mu_p(cm^2/Vs)}$	10	10	1×10^{-4}

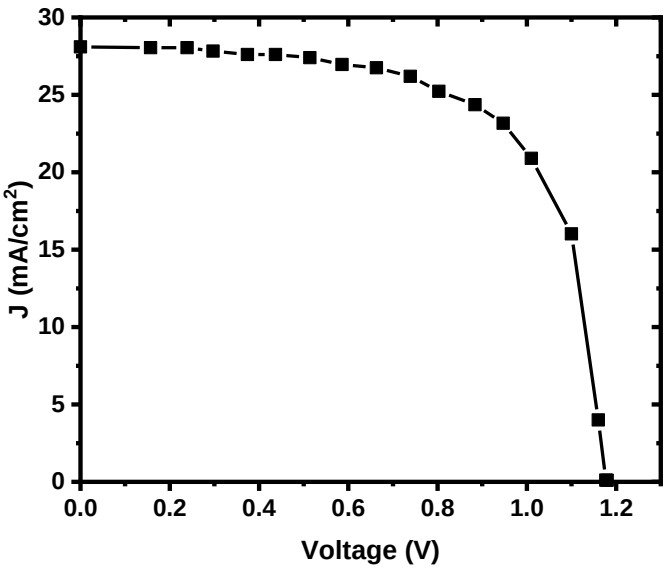

Figure III.6: J-V characteristics of primary PSC solar cell's structure.

The electrical outputs of the primary PSC solar cell are the short-circuit current density Jsc, the open-circuit voltage Voc, the fill factor FF and the conversion efficiency ηare 27.91 mA/cm^2, 1.08 V, 0.72 and 17.77 %, respectively.Good agreement with experimental data was found for our results which are in the measured range of [107] and [108].

III.6 Effect of replacing a PEDOT: PSS by CuScN material

Recent advances in large-area optoelectronics research have demonstrated the tremendous potential of copper(I) thiocyanate (CuSCN) as a universal hole-transport interlayer material for numerous applications, including, transparent thin-film transistors, high-efficiency organic and hybrid organic-inorganic photovoltaic cells, and organic light-emitting diodes (OLEDs). CuSCN combines intrinsic hole-transport (p-type) characteristics with a large bandgap (>3.2 eV) which facilitates optical transparency across the visible to near infrared part of the electromagnetic spectrum. Furthermore, CuSCN is readily available from commercial sources while it is inexpensive and can be processed at low-temperatures using solution-based techniques. This unique combination of desirable characteristics makes CuSCN a promising material for application in emerging large-area optoelectronics.

Early research on CuSCN explored its photocatalytic properties [106], as well as its use in the generation of dye-sensitized photocurrents [107]. While the electronic band structure of p-CuSCN limits its suitability as a photocathode, the adsorption of dye molecules at the semiconductor surface modifies the spectral response of the composite system and amplifies photoresponsivity. Unlike semi-metallic HTL materials such as PEDOT: PSS, CuSCN is an intrinsic semiconductor and as such facilitates excellent electron blocking which can help to minimize exciton recombination at the anode side. Because of its attractive properties, CuSCN has been used as a transparent hole conductor in solid-state inorganic photovoltaic cells, including cells that employ an extremely thin absorber, as well as in quantum.

The perovskite solar cell simulated structure is built (shown in Figure.III.4) using PSCs that have been generated experimentally [107].In this subsection we utilized FTO as ETM and changed the material of HTM were placing a PEDOT: PSS by CuScN. The simulation is carried out under AMG 1.5 solar spectrum with an incident power density of 100 / $mW\,cm^2$ at room temperature

(300 *K)*. Where, the input parameters of FTO are extracted from [107]. The perovskites and CuScN parameters are taken from [108, 109] and [110], respectively. The input parameters of the structure and the different materials are summarized in (Table III.8) and (Figure.III.7) present the effect of replacing a PEDOT: PSS by CuScN material on J-V characteristics of perovskite solar cell solar cell.

Table III.8: Input parameters of MAPbI3 perovskite solar cell.

	ETM(TiO_2)	**Perovskite**	**HTM(CuScN)**
d(µm)	0.1	1.9	0.2
E_g(eV)	3.2	1.55	3.4
χ(eV)	4.1	3.9	1.9
$\boldsymbol{\varepsilon_r}$	9	6.5	9
$\boldsymbol{N_c(cm^{-3})}$	2×10^{18}	2.2×10^{18}	1.7×10^{19}
$\boldsymbol{N_v(cm^{-3})}$	1×10^{18}	1.8×10^{19}	2.5×10^{21}
$\boldsymbol{N_d(cm^{-3})}$	2×10^{18}	5.21×10^{9}	0.0
$\boldsymbol{N_a(cm^{-3})}$	1×10^{17}	5.21×10^{9}	1×10^{18}
$\boldsymbol{\mu_n(cm^2/Vs)}$	300	40	1×10^{-4}
$\boldsymbol{\mu_p(cm^2/Vs)}$	10	10	1×10^{-1}

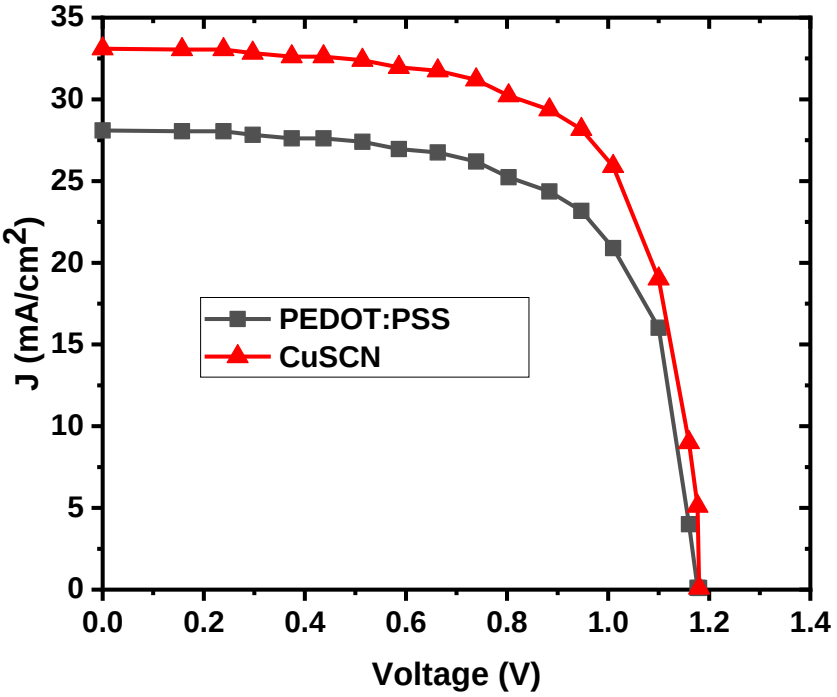

Figure III.7: Effect of replacing a PEDOT: PSS by CuScN material on J-V characteristics of perovskite solar cell solar cell.

As shown in Figure.III.7 a slight improvement is noticed in J-V characteristics of perovskite solar cell solar cell. The CuSCN exhibited the best efficiency even if PEDOT: PSS exhibits the best band alignment. This is due to the holes mobility in PEDOT: PSS which is much smaller than holes mobility in CuSCN. When CuSCN is used as HTM. In this case, the solar cell exhibits a conversion efficiency of 23.30% and a high fill factor of FF 83.70%.

III.7 Effect of CuScN (HTM) Doping Concentrations

During the proposed solar cell simulation, all the input variables of the basic PSC are constant. To study the effect of the CuSCN layer's doping concentration on the perovskite solar cell parameters we varied the CuSCN layer's doping concentration from 10^{14} cm^{-3} to 10^{22} cm^{-3}.

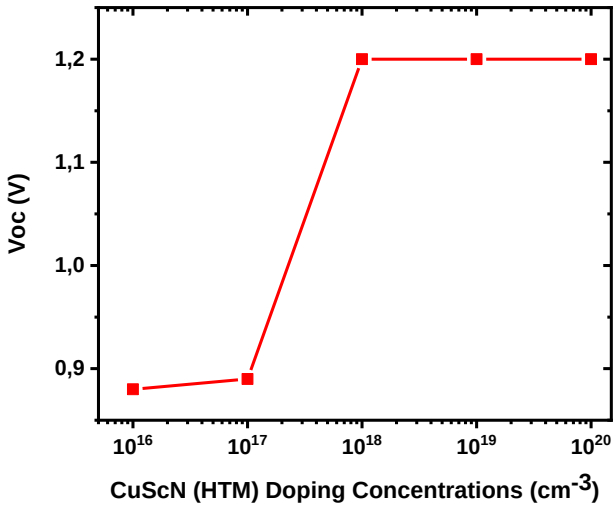

Figure III.8: Effect of the doping concentration of CuScN layer on the Voc of perovskite solar cell solar cell.

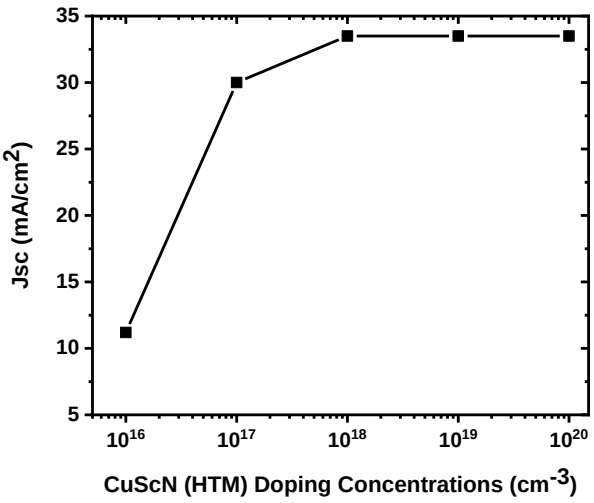

Figure III.9: Effect of the doping concentration of CuScN layer on the Jsc, of perovskite solar cell solar cell.

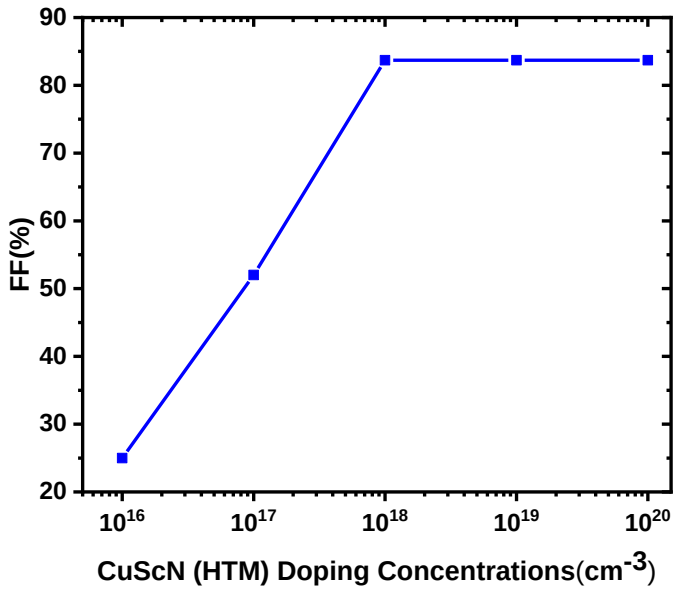

Figure III.10: Effect of the doping concentration of CuScN layer on the FF, of perovskite solar cell solar cell.

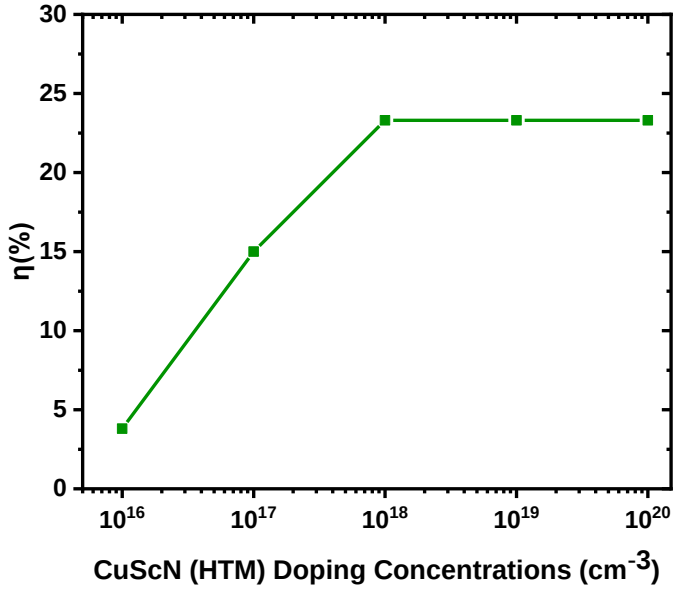

Figure III.11: Effect of the doping concentration of CuScN layer on the η, of perovskite solar cell solar cell.

As the doping concentration of the CuScN layer increases, Jsc increases gradually, as shown in Figure III.8 and Figure III.9 indicates that Voc increases with an increase in CuScN doping concentration and a similar pattern is also observed for FF and efficiency as reflected in Figure III.10 and Figure III.11, respectively. The increase of all the parameters (Voc, Jsc, FF, and efficiency) can be explained by high CuScN doping concentration provides a robust electric field at the interface of perovskite/CuScN interface, which prevents the movement towards the interface of minority electrons which results in a decrease in interface recombination.

Through the curves, we can say that the higher the doping concentration, the higher the electrical characteristics of the solar cell, so we can say that the relationship between them is direct.

III.8 Conclusion

This study is an optimization of a perovskite solar cell with an n-i-p configuration using SILVACO simulator. ITO/Perovskite/PEDOT: PSS structure was the primary modelled solar cell. In this chapter we have studied the perovskite solar cell, first, we studied the electrical characteristics (I-V) of the HTM PEDOT: PSS cell, after that, we replaced PEDOT: PSS (HTM) with CuSCN material and we made a comparison between them, through the obtained results we noticed that the CuSCN material improved the characteristics(I-V) of the perovskite solar cell and we also studied doping concentration of CuSCN (HTM) material to see its effect on the electrical properties of the perovskite solar cell.

Final Conclusion

Conclusion

Solar energy is one of the most important renewable energy sources that reaches the earth's surface by solar radiation, which can be converted by photovoltaic cells.

Solar radiation has several uses in generating heat and electrical energy, in addition to some other services. Among the advanced essential technologies in the field of solar radiation or solar energy are solar cells, which in turn convert sunlight into electrical energy directly.

These cells consist of semiconductors, including silicon, and they do not contain moving parts. The principle of their work is that the semiconductor material absorbs light into direct electricity by photovoltaic action, which we can benefit from in many fields, including lighting, and water pumping……

Currently, the energy crisis is the biggest challenge facing the world today. Solar Batteries have the potential to overcome the energy crisis problem. Over the past 10 years, perovskite solar cells Materials scientists are attracted by their excellent photovoltaic performance and simple manufacturing process. High-efficiency perovskite solar cells use MAPbX3 as a light absorbent layer. This affects the photovoltaic performance of the perovskite solar cells Absorbing or electron transporting layer present. Formerly different species of Electron transport layers have been extensively studied to enhance the performance of MAPbX3-based perovskite solar cells; Up to 24% of PCEs are certified NREL targets MAPbX3-based perovskite solar cell devices. This excellent PCE is close to commercial silicon-based solar cells. Therefore, it can be said that perovskite solar cells can meet our requirements for future energy needs.

Numerical simulation is a key technique for gaining insight into the operating mechanism of solar cells and predicting the maximum values of solar cells with controlled designs. The technique can also provide hints for the structural optimization of different devices.

In this work, we conducted a study of the effect of CuScN material on the electrical properties of the solar cell using the Silvaco Atlas program, which is a semiconductor device simulator based on the principles of 2D and 3D physics, which means that you can predict the electrical properties associated with specific physical structures and polarization conditions.

Through this simulation, we obtained a set of results and curves related to the electrical properties of the solar cells, through which we can say that the CuScN material improved the electrical properties of the perovskite solar cell.

References

References

[1] Zhang, L.; Liu, X.; Li, J.; McKechnie, S. Interactions between molecules and perovskites in halide perovskite solar cells. *Sol. Energy Mater. Sol. Cells* **2018**, *175*, 1–19.

[2] Yang, D.; Yang, R.; Wang, K.; Wu, C.; Zhu, X.; Feng, J.; Ren, X.; Fang, G.; Priya, S.; Liu, S.F. High efficiency planar-type perovskite solar cells with negligible hysteresis using EDTA-complexed SnO2. *Nat. Commun.* **2018**, *9*, 1–11.

[3] Ibn-Mohammed, T.; Koh, S.C.L.; Reaney, I.M.; Acquaye, A.; Schileo, G.; Mustapha, K.B.; Greenough, R. Perovskite solar cells: An integrated hybrid lifecycle assessment and review in comparison with other photovoltaic technologies. *Renew. Sustain. Energy Rev.* **2017**, *80*, 1321–1344.

[4] Green, M.A.; Ho-Baillie, A.; Snaith, H.J. The emergence of perovskite solar cells. *Nat. Photonics* **2014**, *8*, 506.

[5] Chen, Q.; De Marco, N.; Yang, Y.; Song, T.-B.; Chen, C.C.; Zhao, H.; Hong, Z.; Zhou, H.; Yang, Y. Under the spotlight: The organic-inorganic hybrid halide perovskite for optoelectronic applications. *Nano Today* **2015**, *10*, 355–396.

[6] Da, Y.; Xuan, Y.; Li, Q. Quantifying energy losses in planar perovskite solar cells. *Sol. Energy Mater. Sol. Cells* **2017**, *174*, 206–213.

[7] Salhi, B.; Wudil, Y.S.; Hossain, M.K.; Al-Ahmed, A.; Al-Sulaiman, F.A. Review of recent developments and persistent challenges in stability of perovskite solar cells. *Renew. Sustain. Energy Rev.* **2018**, *90*, 210–222.

[8] Kim, H.S.; Lee, C.R.; Im, J.H.; Lee, K.B.; Moehl, T.; Marchioro, A.; Moon, S.J.; Humphry-Baker, R.; Yum, J.H.; Moser, J.E.; et al. Lead iodide perovskite sensitized all-solid-state submicron thin film mesoscopic solar cell with efficiency exceeding 9%. *Sci. Rep.* **2012**, *2*, 1-7.

[9] Kojima, A.; Teshima, K.; Shirai, Y.; Miyasaka, T. Cells, Organometal Halide Perovskites as Visible-Light Sensitizers for Photovoltaic. *J. Am. Chem. Soc.* **2009**, *131*, 6050–6051.

[10] Sun, X.; Zhao, D.; Li, Z. Recent advances in the design of dopant-free hole transporting materials for highly efficient perovskite solar cells. *Chin. Chem. Lett.* **2018**, *29*, 219–231.

[11] Hawash, Z.; Universitet, K.; Ono, L.K.; Qi, Y. Recent Advances in Spiro-MeOTAD Hole Transport Material and Its Applications in Organic-Inorganic Halide Perovskite Solar Cells. *Adva* **2017**, *5*.

[12] Galatopoulos, F.; Savva, A.; Papadas, I.T.; Choulis, S.A. The effect of hole transporting

References

layer in charge accumulation properties of p-i-n perovskite solar cells. *APL Mater.* **2017**, *5*, 1–8.

[13] Uribe, J.; Ramirez, D.; Osorio-Guillen, J.; Osorio, J.; Jaramilo, F. CH3NH3CaI3 Perovskite: Synthesis, Characterization, and First-Principles Studies. *J. Phys. Chem.* **2016**, *120*, 16393–16398.

[14] Zhao, X.; Wang, M. Organic hole-transporting materials for efficient perovskite solar cells. *Mater. Today Energy* **2018**, *7*, 208–220.

[15] Yang, X.; Wang, H.; Cai, B.; Yu, Z.; Sun, L. Progress in hole-transporting materials for perovskite solar cells. *J. Energy Chem.* **2018**, *27*, 650–672.

[16] Chen, W.-Y.; Deng, L.-L.; Dai, S.-M.; Wang, X.; Tian, C.-B.; Zhan, X.-X.; Xie, S.-Y.; Huang, R.-B.; Zheng, L.-S. Low-cost solution-processed copper iodide as an alternative to PEDOT:PSS hole transport layer for efficient and stable inverted planar heterojunction perovskite solar cells. *J. Mater. Chem. A* **2015**, *3*, 19353–19359.

[17] Sun, J.; Lu, J.; Li, B.; Jiang, L.; Chesman, A.S.R.; Scully, A.D.; Gengenbach, T.R.; Cheng, Y.B.; Jasieniak, J.J. Inverted perovskite solar cells with high fill-factors featuring chemical bath deposited mesoporous NiO hole transporting layers. *Nano Energy* **2018**, *49*, 163–171.

[18] Yang, Y.; Pham, N.D.; Yao, D.; Zhu, H.; Yarlagadda, P.; Wang, H. Inorganic p-type semiconductors and carbon materials based hole transport materials for perovskite solar cells. *Chin. Chem. Lett.* **2018**, *29*, 1242–1250.

[19] Christians, J.A.; Fung, R.C.M.; Kamat, P.V. An Inorganic Hole Conductor for Organo-Lead Halide Perovskite Solar Cells. Improved Hole Conductivity with Copper Iodide. *J. Am. Chem. Soc.* **2014**, *136*, 758–764.

[20] Sun, W.; Ye, S.; Rao, H.; Li, Y.; Liu, Z.; Xiao, L.; Chen, Z.; Bian, Z.; Huang, C. Room-Temperature and Solution-Processed Copper Iodide as Hole Transport Layer for Inverted Planar Perovskite Solar Cells. *Nanoscale* **2016**, *8*, 15954–15960.

[21] Li, M.H.; Yum, J.H.; Moon, S.J.; Chen, P. Inorganic p-type semiconductors: Their applications and progress in dye-sensitized solar cells and perovskite solar cells. *Energies* **2016**, *9*, 331.

[22] Han, G.; Du, W.H.; An, B.L.; Bruno, A.; Leow, S.W.; Soci, C.; Zhang, S.; Mhaisalkar, S.G.; Mathews, N. Nitrogen doped cuprous oxide as low cost hole-transporting material for perovskite solar cells. *Scr. Mater.* **2018**, *153*, 104–108.

[23] Chen, J.; Park, N.-G. Inorganic Hole Transporting Materials for Stable and High Efficiency

References

Perovskite Solar Cells. *J. Phys. Chem. C* **2018**, *122*, 14039–14063.

[24] Jaffe, J.E.; Kaspar, T.C.; Droubay, T.C.; Varga, T.; Bowden, M.E.; Exarhos, G.J. Electronic and Defect Structures of CuSCN. *J. Phys. Chem. C* **2010**, *114*, 9111–9117.

[25] Cho, A.; Park, N. Impact of Interfacial Layers in Perovskite Solar Cells. *ChemSusChem* **2017**, *10*, 3687–3704.

[26] Abrusci, A.; Stranks, S.D.; Docampo, P.; Yip, H.; Jen, A.K.; Snaith, H.J. High-Performance Perovskite-Polymer Hybrid Solar Cells via Electronic Coupling with Fullerene Monolayers. *Nano Lett.* **2013**, *13*, 3124–3128.

[27] Jeng, J.; Chiang, Y.; Lee, M.; Peng, S.; Guo, T.; Chen, P.; Wen, T. CH3NH3PbI3 Perovskite/Fullerene Planar-Heterojunction Hybrid Solar Cells. *Adv. Mater.* **2013**, *25*, 3727–3732.

[28] Wang, Y.K.; Jiang, Z.Q.; Liao, L.S. New advances in small molecule hole-transporting materials for perovskite solar cells. *Chin. Chem. Lett.* **2016**, *27*, 1293–1303.

[29] Calió, L.; Kazim, S.; Grätzel, M.; Ahmad, S. Hole-Transport Materials for Perovskite Solar Cells. *Angew. Chem.-Int. Ed.* **2016**, *55*, 14522–14545.

[30] Dhingra, P.; Singh, P.; Rana, P.J.S.; Garg, A.; Kar, P. Hole-Transporting Materials for Perovskite-Sensitized Solar Cells. *Energy Technol.* **2016**, *4*, 891–938.

[31] Bui, T.; Ulfa, M.; Maschietto, F.; Ottochian, A.; Nghiêm, M.; Cio, I.; Goubard, F.; Pauporté, T. Design of dendritic core carbazole-based hole transporting materials for effi cient and stable hybrid perovskite solar cells. *Org. Electron.* **2018**, *60*, 22–30.

[32] Vivo, P.; Salunke, J.K.; Priimagi, A. Hole-Transporting Materials for Printable Perovskite Solar Cells. *Materials* **2017**, *10*, 1087.

[33] Jiang, X.; Yu, Z.; Zhang, Y.; Lai, J.; Li, J.; Gurzadyan, G.G.; Yang, X.; Sun, L. High-Performance Regular Perovskite Solar Cells Employing Low-Cost Poly (ethylenedioxythiophene) as a Hole-Transporting Material. *Sci. Total Environ.* **2017**, *7*, 1–9.

[34] Mahmood, K.; Sarwar, S.; Mehran, M.T. Current status of electron transport layers in perovskite solar cells: materials and properties. *RSC Adv.* **2017**, *7*, 17044–17062.

[35] Yu, Z.; Sun, L. Inorganic Hole-Transporting Materials for Perovskite Solar Cells. *Small Methods* **2017**, *2*, 1–6.

[36] Premalal, E.V.A.; Kannangara, Y.Y.; Ratnayake, S.P.; Nalin de Silva, K.M. Facile Synthesis of Colored and Conducting CuSCN Composite Coated with CuS Nanoparticles. *Nanoscale Res. Lett.* **2017**, *12*, 1–7.

References

[37] Ezealigo, B.N.; Nwanya, A.C.; Simo, A.; Bucher, R.; Osuji, R.U.; Maaza, M.; Reddy, M.V.; Ezema, F.I. A study on solution deposited CuSCN thin films: Structural, electrochemical, optical properties. *Arab. J. Chem.* **2017**.

[38] Pattanasattayavong, P.; Promarak, V.; Anthopoulos, T. Electronic Properties of Copper (I) Thiocyanate (CuSCN). *Adv. Electron. Mater.* **2017**, *3*, 1–32.

[39] Ding, T.; Wang, N.; Wang, C.; Wu, X.; Liu, W.; Zhang, Q.; Fan, W.; Sun, X.W. Solution-processed inorganic copper(i) thiocyanate as a hole injection layer for high-performance quantum dot-based light-emitting diodes. *RSC Adv.* **2017**, *7*, 26322–26327.

[40] Zhang, Q.; Guo, H.; Feng, Z.; Lin, L.; Zhou, J.; Lin, Z. Electrochimica Acta n-ZnO nanorods/p-CuSCN heterojunction light-emitting diodes fabricated by electrochemical method. *Electrochim. Acta* **2010**, *55*, 4889–4894.

[41] Petti, L.; Pattanasattayavong, P.; Lin, Y.H.; Münzenrieder, N.; Cantarella, G.; Yaacobi-Gross, N.; Yan, F.; Tröster, G.; Anthopoulos, T.D. Solution-processed p-type copper(I) thiocyanate (CuSCN) for low-voltage flexible thin-film transistors and integrated inverter circuits. *Appl. Phys. Lett.* **2017**, *110*, 1–5.

[42] Yang, I.S.; Sohn, M.R.; Sung, S.D.; Kim, Y.J.; Yoo, Y.J.; Kim, J.; Lee, W.I. Formation of pristine CuSCN layer by spray deposition method for efficient perovskite solar cell with extended stability. *Nano Energy* **2017**, *32*, 414–421.

[43] Bakr, Z.H.; Wali, Q.; Fakharuddin, A.; Schmidt-Mende, L.; Brown, T.M.; Jose, R. Advances in hole transport materials engineering for stable and e ffi cient perovskite solar cells. *Nano Energy* **2017**, *34*, 271–305.

[44] Madhavan, V.E.; Zimmermann, I.; Roldán-Carmona, C.; Grancini, G.; Buffiere, M.; Belaidi, A.; Nazeeruddin, M.K. Copper Thiocyanate Inorganic Hole-Transporting Material for High-Efficiency Perovskite Solar Cells. *ACS Energy Lett.* **2016**, *1*, 1112–1117.

[45] Hatch, S.M.; Briscoe, J.; Dunn, S. Improved CuSCN–ZnO diode performance with spray deposited CuSCN. *Thin Solid Films* **2013**, *531*, 404–407.

[46] Xiong, Q.; Tian, H.; Zhang, J.; Han, L.; Lu, C.; Shen, B.; Zhang, Y.; Zheng, Y.; Lu, C.; Zeng, Z.; et al. CuSCN modified PEDOT:PSS to improve the efficiency of low temperature processed perovskite solar cells. *Org. Electron.* **2018**, *61*, 151–156.

[47] Chaudhary, N.; Chaudhary, R.; Kesari, J.P.; Patra, A. An eco-friendly and inexpensive solvent for solution processable CuSCN as a hole transporting layer in organic solar cells. *Opt. Mater.* **2017**, *69*, 367–371.

References

[48] Qin, P.; Tanaka, S.; Ito, S.; Tetreault, N.; Manabe, K.; Nishino, H.; Nazeeruddin, M.K.; Grätzel, M. Inorganic hole conductor-based lead halide perovskite solar cells with 12.4% conversion efficiency. *Nat. Commun.* **2014**, *5*, 1–6.

[49] Sepalage, G.A.; Meyer, S.; Pascoe, A.R.; Scully, A.D.; Bach, U.; Cheng, Y.B.; Spiccia, L. A facile deposition method for CuSCN: Exploring the influence of CuSCN on J-V hysteresis in planar perovskite solar cells. *Nano Energy* **2017**, *32*, 310–319.

[50] Qiu, L.; Ono, L.K.; Qi, Y. Advances and challenges to the commercialization of organic–inorganic halide perovskite solar cell technology. *Mater. Today Energy* **2018**, *7*, 169–189.

[51] Ramírez, D.; Riveros, G.; Álvarez, K.; González, B.; Pereyra, C.J.; Dalchiele, E.A.; Marotti, R.E.; Ariosa, D.; Martín, F.; Ramos-barrado, J.R. Electrochemical synthesis of CuSCN nanostructures, tuning the morphological and structural characteristics: From nanorods to nanostructured layers. *Mater. Sci. Semicond. Process.* **2017**, *68*, 226–237.

[52] Shlenskaya, N.N.; Tutantsev, A.S.; Belich, N.A.; Goodilin, E.A.; Grätzel, M.; Tarasov, A.B. Electrodeposition of porous CuSCN layers as hole-conducting material for perovskite solar cells. *Mendeleev Commun.* **2018**, *28*, 378–380.

[53] Murugadoss, G.; Thangamuthu, R.; Senthil Kumar, S.M. Fabrication of CH3NH3PbI3 perovskite-based solar cells: Developing various new solvents for CuSCN hole transport material. *Sol. Energy Mater. Sol. Cells* **2017**, *164*, 56–62.

[54] Wang, F.; Chen, D.; Hu, Z.; Qin, L.; Sun, X.; Huang, Y. In situ decoration of CuSCN nanorod arrays with carbon quantum dots for highly ef fi cient photoelectrochemical performance. *Carbon* **2017**, *125*, 344–351.

[55] Wu, W.; Cui, S.; Yang, C.; Hu, G.; Wu, H. Electrochemistry Communications Electrochemically superfilling of n-type ZnO nanorod arrays with p-type CuSCN semiconductor. *Electrochem. Commun.* **2009**, *11*, 1736–1739.

[56] Chappaz-Gillot, C.; Salazar, R.; Berson, S.; Ivanova, V. Insights into CuSCN nanowire electrodeposition on flexible substrates. *Electrochim. Acta* **2013**, *110*, 375–381.

[57] Lv, Y.; Guo, Y.; Zhang, H.; Zhou, X.; Chen, H. Enhanced efficiency and stability of fully air-processed TiO2 nanorods array based perovskite solar cell using commercial available CuSCN and carbon. *Sol. Energy* **2018**, *173*, 7–16.

[58] Karuppuchamy, S.; Murugadoss, G.; Ramachandran, K.; Saxena, V.; Thangamuthu, R. Inorganic based hole transport materials for perovskite solar cells. *J. Mater. Sci. Mater. Electron.* **2018**, *29*, 8847–8853.

References

[59] Zhao, K.; Munir, R.; Yan, B.; Yang, Y.; Kim, T.; Amassian, A. Solution-processed inorganic copper(i) thiocyanate (CuSCN) hole transporting layers for efficient p-i-n perovskite solar cells. *J. Mater. Chem. A* **2015**, *3*, 20554–20559.

[60] Chowdhury, T.H.; Akhtaruzzaman, M.; Kayesh, M.E.; Kaneko, R.; Noda, T.; Lee, J.J.; Islam, A. Low temperature processed inverted planar perovskite solar cells by r-GO/CuSCN hole-transport bilayer with improved stability. *Sol. Energy* **2018**, *171*, 652– 657.

[61] Wijeyasinghe, N.; Regoutz, A.; Eisner, F.; Du, T.; Tsetseris, L.; Lin, Y.H.; Faber, H.; Pattanasattayavong, P.; Li, J.; Yan, F.; et al. Copper(I) Thiocyanate (CuSCN) Hole-Transport Layers Processed from Aqueous Precursor Solutions and Their Application in Thin-Film Transistors and Highly Efficient Organic and Organometal Halide Perovskite Solar Cells. *Adv. Funct. Mater.* **2017**, *27*, 1–13.

[62] Song, Z.; Phillips, A.B.; Heben, M.J.; Song, Z.; Watthage, S.C.; Phillips, A.B.; Heben, M.J.; Song, Z.; Watthage, S.C.; Phillips, A.B. Pathways toward high-performance perovskite solar cells: Review of recent advances in organo-metal halide perovskites for photovoltaic applications. *J. Photonics Energy* **2016**, *6*, 022001.

[63] Ito, S.; Tanaka, S.; Vahlman, H.; Nishino, H.; Manabe, K.; Lund, P. Carbon-Double-Bond-Free Printed Solar Cells from TiO2/CH3NH3PbI3/CuSCN/Au: Structural Control and Photoaging Effects. *ChemPhysChem* **2014**, *15*, 1194–1200.

[64] Yao, Y.; Wang, G.; Liao, L.; Liu, D.; Zhou, G.; Xu, C.; Yang, X.; Wu, R.; Song, Q. Enhancing the open circuit voltage of PEDOT:PSS-PC61BM based inverted planar mixed halide perovskite solar cells from 0.93 to 1.05 V by simply oxidizing PC61 BM. *Org. Electron.* **2018**, *59*, 260–265.

[65] Han, J.; Tu, Y.; Liu, Z.; Liu, X.; Ye, H.; Tang, Z.; Shi, T.; Liao, G. Efficient and stable inverted planar perovskite solar cells using dopant-free CuPc as hole transport layer. *Electrochim. Acta* **2018**, *273*, 273–281

[66] Guo, H.; Huang, X.; Pu, B.; Yang, J.; Chen, H.; Zhou, Y.; Yang, J.; Li, Y.; Wang, Z.; Niu, X. Efficiency enhancement in inverted planar perovskite solar cells by synergetic effect of sulfated graphene oxide (sGO) and PEDOT:PSS as hole transporting layer. *RSC Adv.* **2017**, *7*, 50410–50419.

[67] Castro, E.; Murillo, J.; Fernandez-delgado, O.; Echegoyen, L. Progress in fullerene-based hybrid perovskite solar cells. *J. Mater. Chem. C* **2018**, *6*, 2635–2651.

[68] Qin, Q.; Zhang, Z.; Cai, Y.; Zhou, Y.; Liu, H.; Lu, X.; Gao, X.; Shui, L.; Wu, S.; Liu, J.

References

Improving the performance of low-temperature planar perovskite solar cells by adding functional fullerene end-capped polyethylene glycol derivatives. *J. Power Sources* **2018**, *396*, 49–56.

[69] Chavhan, S.; Miguel, O.; Grande, H.J.; Gonzalez-Pedro, V.; Sánchez, R.S.; Barea, E.M.; Mora-Seró, I.; Tena-Zaera, R. Organo-metal halide perovskite-based solar cells with CuSCN as the inorganic hole selective contact. *J. Mater. Chem. A* **2014**, *2*, 12754–12760.

[70] Arora, N.; Dar, M.I.; Hinderhofer, A.; Pellet, N.; Schreiber, F.; Zakeeruddin, S.M.; Grätzel, M. Perovskite solar cells with CuSCN hole extraction layers yield stabilized efficiencies greater than 20%. *Science* **2017**, *358*, 768–771.

[71] Baranwal, A.K.; Kanda, H.; Shibayama, N.; Ito, S. Fabrication of fully non-vacuum processed perovskite solar cells using inorganic CuSCN hole-transporting material and carbon- back contact. *Sustain. Energy Fuels* **2018**.

[72] Ye, S.; Sun, W.; Li, Y.; Yan, W.; Peng, H.; Bian, Z.; Liu, Z.; Huang, C. CuSCN-Based Inverted Planar Perovskite Solar Cell with an Average PCE of 15.6%. *Nano Lett.* **2015**,*15*, 3723–3728.

[73] Hu, W.; Dall'Agnese, C.; Wang, X.-F.; Chen, G.; Li, M.-Z.; Song, J.-X.; Wei, Y.-J.; Miyasaka, T. Copper iodide-PEDOT:PSS double hole transport layers for improved efficiency and stability in perovskite solar cells. *J. Photochem. Photobiol. A Chem.* **2018**, *357*, 36–40.

[74] Wang, H.; Yu, Z.; Lai, J.; Song, X.; Yang, X.; Hagfeldt, A.; Sun, L. One plus one greater than two: high-performance inverted planar perovskite solar cells based on a composite CuI/CuSCN hole-transporting layer. *J. Mater. Chem. A* **2018**, *6*, 21435–21444.

[75] Jung, M.; Kim, Y.C.; Jeon, N.J.; Yang, W.S.; Seo, J.; Noh, J.H.; Il Seok, S. Thermal Stability of CuSCN Hole Conductor-Based Perovskite Solar Cells. *ChemSusChem* **2016**, *9*, 1–6.

[76] Lyu, M.; Chen, J.; Park, N. Improvement of e ffi ciency and stability of CuSCN-based inverted perovskite solar cells by post-treatment with potassium thiocyanate. *J. Solid State Chem.* **2019**, *269*, 367–374.

[77] Yang, W.S.; Park, B.W.; Jung, E.H.; Jeon, N.J.; Kim, Y.C.; Lee, D.U.; Shin, S.S.; Seo, J.; Kim, E.K.; Noh, J.H.; et al. Il Iodide management in formamidinium-lead-halide-based perovskite layers for efficient solar cells. *Science* **2017**, *356*, 1376–1379.

[78] Park, J.H.; Seo, J.; Park, S.; Shin, S.S.; Kim, Y.C.; Jeon, N.J.; Shin, H.W.; Ahn, T.K.; Noh,

References

J.H.; Yoon, S.C.; et al. Il Efficient CH3NH3PbI3 Perovskite Solar Cells Employing Nanostructured p-Type NiO Electrode Formed by a Pulsed Laser Deposition. *Adv. Mater.* **2015**, *27*, 4013–4019.

[79] Duong, T.; Peng, J.; Walter, D.; Xiang, J.; Shen, H.; Chugh, D.; Mark, N.; Zhong, D.; Li, J.; Weber, K.J.; et al. Perovskite Solar Cells Employing Copper Phthalocyanine Hole Transport Material with an Efficiency over 20% and Excellent Thermal Stability. *ACS Energy Lett.* **2018**, *3*, 2441–2448.

[80] Wu, Y.; Xie, F.; Chen, H.; Yang, X.; Su, H.; Cai, M.; Zhou, Z.; Noda, T.; Han, L. Thermally Stable MAPbI3 Perovskite Solar Cells with Efficiency of 19.19% and Area over 1 cm2 achieved by Additive Engineering. *Adv. Mater.* **2017**, *29*, 1–8.

[81] Chen, J.; Cai, X.; Yang, D.; Song, D.; Wang, J.; Jiang, J.; Ma, A.; Lv, S.; Hu, M.Z.; Ni, C. Recent progress in stabilizing hybrid perovskites for solar cell applications. *J. Power Sources* **2017**, *355*, 98–133.

[82] Yu, H.; Wu, Z.; Huang, X.; Shi, S.; Li, Y. Synergetic effects of acid treatment and localized surface plasmon resonance in PEDOT:PSS layers by doping HAuCl4 for efficient polymer solar cells. *Org. Electron.* **2018**, *62*, 121–132.

[83] Lee, J.J.; Lee, S.H.; Kim, F.S.; Choi, H.H.; Kim, J.H. Simultaneous enhancement of the efficiency and stability of organic solar cells using PEDOT:PSS grafted with a PEGME buffer layer. *Org. Electron.* **2015**, *26*, 191–199.

[84] Meyer, E.; Mutukwa, D.; Zingwe, N.; Taziwa, R. Lead-Free Halide Double Perovskites: A Review of the Structural, Optical, and Stability Properties asWell as Their Viability to Replace Lead Halide Perovskites. *Metals* **2018**, *3*, 667.

[85] D.-Y. Son, J.-H. Im, H.-S. Kim, N.-G. Park, 11% efficient perovskite solar cell based on ZnO nanorods: an effective charge collection system, J. Phys. Chem. C 118 (2014) 16567–16573.

[86] N.J. Jeon, J.H. Noh, W.S. Yang, Y.C. Kim, S. Ryu, J.W. Seo, S.I. Seok, Compositional engineering of perovskite materials for high-performance solar cells, Nature 517 (2015) 476–480.

[87] A. Hima, N. Lakhdar, A. Saadoune, Effect of electron transporting layer on power conversion efficiency of perovskite-based solar cell: comparative study, J. Nano Electron. Phys. 11 (2019), 01026-1-3.

References

[88] A. Hima, N. Lakhdar, B. Benhaoua, A. Saadoune, I. Kemerchou, F. Rogti, An optimized perovskite solar cell designs for high conversion efficiency, Superlattice Microstruct. 129 (2019) 240–246.

[89] A. Kojima, K. Teshima, Y. Shirai, T. Miyasaka, Organometal halide perovskites as visible-light sensitizers for photovoltaic cells, J. Am. Chem. Soc. 131 (2009) 6050–6051.

[90] National Renewable Energy Laboratory, Best research-cell efficiencies. https://www.nrel.gov/pv/assets/pdfs/best-research-cell efficiencies.20190802. pdf.

[91] B. Conings, J. Drijkoningen, N. Gauquelin, A. Babayigit, J. D'Haen, L. D'Olieslaeger, A. Ethirajan, J. Verbeeck, J. Manca, E. Mosconi, others, Intrinsic thermal instability of methylammonium lead trihalide perovskite, Adv. Energy Mater. 5 (2015) 1500477.

[92] P.-P. Sun, Q.-S. Li, L.-N. Yang, Z.-S. Li, Theoretical insights into a potential lead-free hybrid perovskite: substituting Pb2þ with Ge2þ, Nanoscale 8 (2016) 1503–1512.

[93] Qiong Wang, Nga Phung, Diego Di Girolamo, Paola Vivo, Antonio Abate, Enhancement in lifespan of halide perovskite solar cells, Energy Environ. Sci. 12 (2019) 865–886.

[94] Rui Wang, Muhammad Mujahid, Yu Duan, Zhao-Kui Wang, Jingjing Xue, Yang Yang, A review of perovskites solar cell stability, Adv. Funct. Mater. (2019), https://doi.org/10.1002/adfm.201808843.

[95] Hang Hu, Binghai Dong, Wei Zhang, Low-toxic metal halide perovskites: opportunities and future challenges, J. Mater. Chem. 5 (2017) 11436–11449.

[12] B. Saparov, D.B. Mitzi, Organic-inorganic perovskites: structural versatility for functional materials design, Chem. Rev. 116 (2016) 4558–4596.

[96] N. Lakhdar, A. Hima, Electron Transport Material Effect on Performance of Perovskite Solar Cells Based on CH3NH3GeI3, Optical Materials, 2019.

[97] Ahmed-Ali Kanoun, Mohammed Benali Kanoun, Abdelkrim E. Merad, Souraya Goumri-Said, Toward development of high-performance perovskite solar cells based on CH3NH3GeI3 using computational approach, Sol. Energy 182 (2019) 237–244.

[98] Yanyan Liu, Zhenlong Zhang, Huiping Gao, Huafang Zhang, Yanli Mao, A novel inorganic hole-transporting material of CuInS2 for perovskite solar cells with high

References

efficiency and improved stability, Org. Electron. 75 (2019) 105430.

[99] C. Devi, R. Mehra, Device simulation of lead-free MASnI3 solar cell with CuSbS 2 (copper antimony sulfide), J. Mater. Sci. 54 (2019) 5615–5624.

[100] P. Qin, S. Tanaka, S. Ito, N. Tetreault, K. Manabe, H. Nishino, M.K. Nazeeruddin, M. Gratzel, € Inorganic hole conductor-based lead halide perovskite solar cells with 12.4% conversion efficiency, Nat. Commun. 5 (2014) 3834–3839.

[101] N.T. Satyala, W.T. Wondmagegn, R.J. Pieper, M.R. Korn, Simulation of Copper Phthalocyanine/Fullerene Heterojunction Photovoltaic Cell with and without Electron Transport Layer, ETL, 2011, https://doi.org/10.1557/PROC-1212-S08-18.

[102] K. Tan, et al., Controllable design of solid-state perovskite solar cells by SCAPS device simulation, Solid State Electron. 126 (2016) 75–80.

[103] Y.-Q. Zhao, et al., Strong ferroelectric polarization of CH 3 NH 3 GeI 3 with highabsorption and mobility transport anisotropy: theoretical study, J. Mater. Chem. C 5 (2017) 5356–5364.

[104] W. Abdelaziz, A. Shaker, M. Abouelatta, A. Zekry, Possible efficiency boosting of non-fullerene acceptor solar cell using device simulation, Opt. Mater. 91 (2017) 239–245.

[105] Device Simulator Atlas Ver. 5.10.0.R. Atlas User's Manual, SILVACO Int., Santa Clara, CA, July (2005)

[106] R. Teimouri, R. Mohammadpour, Potential application of CuSbS2 as the hole transport material in perovskite solar cell: a simulation study, Superlattice Microstruct. 118 (2018) 116–122.

[107] P. Pattanasattayavong, et al., Electric field-induced hole transport in copper (I) thiocyanate (CuSCN) thin-films processed from solution at room temperature, Chem. Commun. 49 (2013) 4154–4156.

[108] Z. Zhu, Y. Bai, X. Liu, C.C. Chueh, S. Yang, A.K.Y. Jen, Enhanced efficiency and stability of inverted perovskite solar cells using highly crystalline SnO2 nanocrystals as the robust electron-transporting layer, Adv. Mater. 28 (2016) 6478–648.

[109] Cao F, Yu D J, Li X M, Zhu Y, Sun Z G, Shen Y L, Wu Y, Wei Y and Zeng H B 2017 *J. Mater. Chem. C* **5** 7441

[110] Ramasamy P, Lim D H, Kim B, Lee S H, Lee M S and Lee J S 2016 *Chem. Commun.* **52** 2067.